NOTICE

The quality of this microform is heavily dependent upon the quality of the original thesis submitted for microfilming. Every effort has been made to ensure the highest quality of reproduction possible.

If pages are missing, contact the university which granted the degree.

Some pages may have indistinct print especially if the original pages were typed with a poor typewriter ribbon or if the university sent us an inferior photocopy.

Reproduction in full or in part of this microform is governed by the Canadian Copyright Act, R.S.C. 1970, c. C-30, and subsequent amendments.

AVIS

La qualité de cette microforme dépend grandement de la qualité de la thèse soumise au microfilmage. Nous avons tout fait pour assurer une qualité supérieure de reproduction.

S'il manque des pages, veuillez communiquer avec l'université qui a conféré le grade.

La qualité d'impression de certaines pages peut laisser à désirer, surtout si les pages originales ont été dactylographiées à l'aide d'un ruban usé ou si l'université nous a fait parvenir une photocopie de qualité inférieure.

La reproduction, même partielle, de cette microforme est soumise à la Loi canadienne sur le droit d'auteur, SRC 1970, c. C-30, et ses amendements subséquents.

TWO-DIMENSIONAL NUMERICAL MODELING

OF ICE COVER LEADING EDGE

Xiu Tao Zhang

A Thesis

in

The Department

of

Civil Engineering

Presented in Partial Fulfilment of the Requirements

for the Degree of Master of Applied Science at

Concordia University

Montreal, Quebec, Canada

March 1992

ISBN 0-315-73615-1

ABSTRACT

Two-Dimensional Numerical Modeling of Ice Cover Leading Edge

Xiu Tao Zhang

The phenomena of the ice melting is the result of the heat transfer between river flow, the atmosphere, and the ice cover. The water temperature beneath river ice covers has the most important influence on the heat flux to the overlying ice cover. To model or simulate the behavior of the ice cover melting, proper estimation of the heat transfer coefficient at water-ice interface is important, because it plays a key role in calculating the heat flux from the river water to the ice cover. Whether the heat flux from water to the ice cover can be calculated precisely depends to large extent on determining accurately the heat transfer coefficient. Most of the empirical equations for predicting the heat transfer coefficient in the literature only apply to the fully developed flow and result in under-estimating the ice melting in the entrance region of the ice cover in the model application. Proper evaluation of the heat transfer coefficient in the entry region is of large interest in modeling the ice cover melting.

The present research aims at studying the effects of the heat transfer coefficient on modeling the ice cover melting, leading to a method that overcomes the under-estimation of ice melting in entrance region in

traditional numerical models application by using a variable heat transfer coefficient. Three empirical approaches for predicting the heat transfer coefficient for ice-covered rivers have been examined and their effects on ice cover melting were compared. A new formula for the evaluation of heat transfer coefficient which varies with the distance in flow direction has been derived to be employed in a numerical model, with goal of a better modeling of ice cover melting near the leading edge. The work was carried out through the application of a two-dimensional numerical model. The results from the computations have been compared to experimental observations and field study.

ACKNOWLEDGEMENT

The successful completion of this research project involves many more people than the author alone. First and foremost, my deepest appreciation goes to Dr. Semaan Sarraf, my thesis supervisor, for his guidance, advice as well as encouragement. His sincere direction is largely responsible for whatever merits this document possesses. I also like to acknowledge the advice and assistance received from the people in our department.

This thesis is dedicated to my parents, Jixuan Zhang and Lianxu Bi, whose love and support have meant everything to me, not only during my years of study, but throughout my whole life.

Last but not least, I wish to express my heartfelt gratitude to my husband, Wei Yan, for his helping, moral support as well as enduring understanding. Without him, this accomplishment would have been impossible.

TABLE OF CONTENTS

LIST OF FIGURES

LIST OF TABLES

LIST OF SYMBOLS

A	=	area of the ice cover, in m^2
a	=	annual variation in solar radiation constant, in J cm^{-2} day^{-1}
b	=	annual variation in solar radiation constant
C	=	cloud cover, in tenths
C_c	=	coefficient for ice cover reduction in convective heat transfer
c	=	empirical constant for atmospheric radiation
c_f	=	drag fraction coefficient
c_{fn}	=	friction factor for rough surface in the entrance region
c_p	=	specific heat of water, in kJ kg^{-1} $^oC^{-1}$
c_n	=	friction correlation factor
D	=	hydraulic diameter, in m
D_o	=	depth of the point of maximum water velocity below the ice cover, in m
D_t	=	total flow depth, in m
D_x	=	dispersion coefficient in x direction, in m^2 s^{-1}
D_y	=	dispersion coefficient in y direction, in m^2 s^{-1}
d	=	empirical constant for atmospheric radiation
e_a	=	air vapor pressure, in mb
e_s	=	saturation vapor pressure, in mb
F	=	conservative variable, in m^3 s^{-2}
f	=	Darcy-Weisbach friction coefficient
G	=	conservative variable, in m^3 s^{-2}
g	=	gravitational acceleration, in m s^{-2}

h = water depth, in m

h_{wi} = heat transfer coefficient from water to ice, in J m^{-2} s^{-1} $^oC^{-1}$

h_x = local heat transfer coefficient, in J m^{-2} s^{-1} $^oC^{-1}$

K_m = Manning's unit conversion factor

k = water thermal conductivity, J m^{-1} s^{-1} $^oC^{-1}$

k_c = empirical constant for atmospheric radiation

k_i = ice thermal conductivity, in J m^{-1} s^{-1} $^oC^{-1}$

k_n = coefficient for free convection

k_x = dispersion constant in x direction

k_y = dispersion constant in y direction

L = length of the ice cover, in m

L_i = ice heat of fusion, in J kg^{-1}

L_t = thermal entry length, in m

L_x = McCormack operator in x direction backward prediction, forward corrector

L_y = McCormack operator in y direction backward prediction, forward corrector

L'_x = McCormack operator in x direction forward prediction, backward corrector

L'_y = McCormack operator in y direction forward prediction, backward corrector

Nu = Nusselt number

Nu_x = local Nusselt number

n = Manning's coefficient

n_b = Manning's coefficient of river bed

n_i = Manning's coefficient of underside of ice cover

n_{ie} = Manning's coefficient of underside of ice cover in the entry region

Pr = Prandtl number

q_{wi} = heat flux from water to ice cover, in J m^{-2} s^{-1}

R = hydraulic radius, in m

Re = Reynolds number

S = conservative variable, in m^{-3} s^{-1}

S_{fx} = friction slope in x direction

S_{fy} = friction slope in y direction

S_{ox} = bed slope in x direction

S_{oy} = bed slope in y direction

St = Stanton number

T = water temperature, in $^oC^{-1}$

T_a = air temperature, in $^oC^{-1}$

T_{ak} = air temperature, in ^oK

T_f = freezing point temperature of water, in $^oC^{-1}$

T_i = ice cover internal temperature, in $^oC^{-1}$

T_s = ice surface temperature, in $^oC^{-1}$

T_{ws} = water surface temperature, in $^oC^{-1}$

T_{sk} = water or ice top surface temperature, in ^oK

T_w = water temperature, in ^oC

t = time, in s

Δt = time step, in s

Δt_2 = one half the time step, in s

U = unit discharge in x direction, in m^2 s^{-1}

U^* = shear velocity in x direction, in m s^{-1}

u = flow velocity in x direction, in m s^{-1}

u_∞ = flow velocity outside boundary layer in x direction, in m s^{-1}

V = unit discharge in y direction, in m^2 s^{-1}

V^* = shear velocity in y direction, in m s^{-1}

V_a = wind velocity at 2 m above surface, in m s^{-1}

v = flow velocity in y direction, in m s^{-1}

x = space coordinate longitudinal direction, in m

x_L = length of an ice cover from the leading edge, in m

Δx = grid spacing in x direction, in m

y = space coordinate transverse direction, in m

Δy = grid spacing in y direction, in m

Z_f = bed elevation, in m

α = surface albedo

α_a = empirical constant for ice surface albedo

α_i = empirical constant for ice surface albedo

β_i = fraction of solar radiation which penetrates ice-water interface

δ = boundary layer thickness

ε = thermal diffusivity, in m^2 s^{-1}

ε_s = emissivity of water or ice surface

θ = ice thickness, in m

$\Delta\theta_s$ = ice thickness change at top surface, in m

θ_t = temperature dimensionless profile

$\Delta\theta_w$ = ice thickness change at bottom surface, in m

θ_∞ = temperature dimensionless outside thermal boundary layer

κ = turbulent kinetic energy

μ = dynamic viscosity, in kg m^{-1} s^{-1}

μ_b = dynamic viscosity at bulk fluid, in kg m^{-1} s^{-1}

μ_w = dynamic viscosity at the wall, in kg m^{-1} s^{-1}

ν_t = turbulent viscosity

ρ = water density, in kg m^{-3}

σ = Stefan-Boltzman constant, in J cm^{-2} day^{-1}

τ = surface shear stress, in kg m^{-2}

τ_i = bulk extinction coefficient, in cm^{-1}

τ_{sx} = surface stress in x direction, in kg s^{-2} m^{-1}

τ_{sy} = surface stress in y direction, in kg s^{-2} m^{-1}

υ = kinetic viscosity, in m^2 s^{-1}

Φ = source term, in ^oC s^{-1}

ϕ = heat transfer to water, in J cm^{-2} day^{-1}

ϕ_b = effective back radiation, in J cm^{-2} day^{-1}

ϕ_{ba} = atmospheric radiation, in J cm^{-2} day^{-1}

ϕ_{bn} = net atmospheric radiation, in J cm^{-2} day^{-1}

ϕ_{bs} = longwave radiation emitted by the river surface, in J cm^{-2} day^{-1}

ϕ_c = conductive heat transfer, in J cm^{-2} day^{-1}

ϕ_e = evapo-condensation flux, in J cm^{-2} day^{-1}

ϕ_{lat} = latitude on earth's surface, in degrees

ϕ_{ri} = incoming shortwave radiation, in J cm^{-2} day^{-1}

ϕ_s = net shortwave radiation, in J cm^{-2} day^{-1}

ϕ_{sp} = shortwave penetration into the water body, in J cm^{-2} day

ψ = empirical constant for ice surface albedo

CHAPTER 1

INTRODUCTION

1.1 Phenomena of Ice Melting

Water bodies in rivers and lakes are frequently utilized to dissipate excess of heat from power plants. The heated effluent discharges may alter the hydrothermal and ecological environment of the aquatic system. In cold regions, where rivers are ice covered for a considerable period of the year, these thermal effluents have the effects of provoking the premature or accelerating the decay of ice covers.

The phenomena of the ice melting is the result of heat transfer between the river flow, the atmosphere, and the ice cover. Heat flows by convection from the water to the ice, and by conduction through the ice cover. It has been widely recognized that the water temperature beneath the river ice cover has an important influence on the heat flux to the overlying ice cover. Even if water temperature is very close to 0°C, the resulting heat flux from water to the overlying ice can still cause significant ice melting. The roughness on the underside of the ice is another main factor influencing the heat flux from water to the ice cover.

1.2 The Problem Considered

To model or simulate the behavior of the ice cover melting, proper estimation of the heat transfer coefficient plays an important role in calculating the heat flux from the water to the ice cover. Whether the heat flux from water to ice cover can be calculated precisely depends to large extent on determining accurately the heat transfer coefficient.

Empirical equations for predicting the heat transfer coefficient as well as the theoretical analyses for evaluating the Nusselt number are not sparse in the literature. The application of these formulas in the computation of heat transfer between water and the ice cover requires a knowledge of the physical properties of the flow. Mostly, these empirical equations are applicable in fully developed flow and the value of the heat transfer coefficient predicted from the empirical equations is constant, resulting in constant heat flux estimation between water and the ice cover, which does not agree with the entry region of the ice cover. In the application of the heat flux from water to the ice cover, the ice cover melting in the entry region is often under-estimated by the empirical formulas. Proper formulation of the heat transfer coefficient in the entry region is of considerable interest in modeling ice cover melting and transient retreat of the leading edge.

1.3 Literature Review

1.3.1 Investigation of Water-Ice Heat Transfer

The subject of river ice cover melting has been studied previously by a number of researchers. Dingman et al. (1967) obtained better agreements with measured ice free reaches using improved relations between the heat loss rate and meteorological conditions. A one-dimensional model of sea ice thermodynamics to simulate heat transfer below, within, and above the ice-snow cover was developed by Maykut & Untersteiner (1971). Hsu (1973) verified the quasi-steadiness of the heat conduction through the ice cover. Paily et al. (1974) solved the one-dimensional energy equation including the effect of longitudinal dispersion in the model. Hewlett (1976) studied the movement of the leading edge of the ice cover through laboratory experiments. A one dimensional model was developed by Ashton (1979) for ice cover suppression under given meteorological conditions. Heat transfer processes as well as varying meteorological conditions were considered. A two-dimensional model for computing an equilibrium surface temperature from energy balance was applied for Lake Erie (Wake & Rumer, 1979). Also a one-dimensional model for St. Lawrence ice cover was developed by Shen-Chiang (1984). Plouffe (1987) employed a two-dimensional numerical model of river ice cover melting due to a side thermal effluent. A two-dimensional model for ice cover melting under turbulent flow conditions was accomplished by Sarraf et al. (1990).

A few studies have also been carried out to predict the heat flux from water to the overlying ice cover in natural rivers (Baines, 1961; Ashton and

Kennedy, 1972; Cowley and Lavender, 1975). Calkins (1984) compared predicted heat flux with field measurements. He found that the heat transfer coefficient computed from field data on both ice cover melting and water temperature attenuation are higher than the values one would compute based on extrapolation of previous laboratory data. Wankiewicz (1984) modeled the growth of river ice during the winter of 1977-1978 for Caribou Creek. Marsh et al. (1986) used different correlations for calculating the heat flux and the results were compared to temperature decay method and field measurement.

1.3.2 Entry Region Influence on Heat Transfer

The thermal entrance region can have influence on the heat transfer process. The heat transfer coefficient varies substantially in this region. White (1984) defined that for laminar flow the local Nusselt number can drop to within 2% of the thermally developed value in the thermal entry length. Ozisik (Ozisik, 1985) defined that the thermal entry region is the length required from the beginning of the heat transfer section to achieve a local Nusselt number equal to 1.05 times the corresponding fully developed value.

Little work appears to be done on predicting the ice melting in the entrance region of the ice cover by using proper heat transfer coefficient. It has already been found that the heat flux is higher in the entry region of the tubes or pipes. Therefore, a few empirical formulas or equations of heat transfer coefficient were derived to be applied in the entry region.

One of the available formulation of the mean Nusselt number for laminar flow in the entrance region is given by Hausen (Ozisik, 1985), but it is only to be used in a circular tube at constant wall temperature for laminar flow. A rather simple empirical correlation has been proposed by Sieder and Tate (1936) to approximate the mean Nusselt number in the entrance region. This correlation is also valid for laminar flow in a circular tube at constant wall temperature. Another form of the correlation for the Nusselt number in the entry region is recommended by Ozisik (Ozisik, 1985) for turbulent flow. However, the relation is applicable only for liquid metals in turbulent flow condition.

Finally, surface roughness effects on heat transfer rate were investigated by a number of researchers. Dipprey and Sabersky (White, 1984) found that roughness can increase heat transfer by a factor up to 2.5.

1.4 Objective And Scope of The Work

The present research aims at studying the effect of heat transfer coefficient on modeling the ice cover melting, with a focus on the entrance region. Three empirical approaches, the Dittus-Boelter, the Colburn and the Petukhov-Popov equations which are commonly used for predicting the heat transfer coefficient for ice-covered rivers, have been studied through the applications of a two-dimensional numerical model. Modeling results were compared to the experimental investigations done by Hewlett (1976) and a field study on the Mississippi River (Ashton, 1980).

Based on the heat and momentum transfer analogy, a new derivation of the heat transfer coefficient has been obtained. The new proposed correction is a function of the distance in the flow direction, producing the largest value at the leading edge and gradually small one downstream. This new correlation produced a closer estimation of the ice melting in the entry region of the ice cover in which the heat transfer coefficient is often under-estimated in ice melting modeling when empirical formulas are used. The new correlation has been tested through the application of the model. The results from the computations have compared well with the experimental observations (Hewlett, 1976).

The computations were carried out through the application of a two-dimensional numerical model. The hydrodynamic fields of channel in the laboratory and Mississippi River were modeled using the depth integrated St. Venant equations for shallow water, incorporating the effect of the ice cover presence on the flow. Inlet water temperature in both cases were also simulated in the model and water temperature distribution was determined from the unsteady depth average energy equation. The laboratory operating conditions and meteorological conditions in the field were reproduced accurately in the model.

The numerical solutions were obtained using a finite difference method. The energy equation for temperature distribution was solved using upwind scheme, while a modified version of the MacCormack scheme was employed to discretize the hydrodynamic equations.

The computational results were compared to the experimental data given by Hewlett (1976) and the field data carried out by the US. Army Cold Regions Research and Engineering Laboratory (Ashton, 1980).

1.5 Outline of The Thesis

The thesis is grouped into five chapters. This chapter is an introduction to the accomplished research. Chapter 2 gives the basic theory of the convective heat transfer between the water and ice cover. Various empirical equations for predicting the heat transfer coefficient, including three equations used in the modeling, are also presented. A new correlation to solve the problem encountered in the entry region of the ice cover is derived and described. A two-dimensional numerical model utilized in the present research is described in chapter 3. The governing equations, the numerical schemes employed as well as the equations for the ice cover used in the model are presented. In chapter 4, descriptions of the procedure of the computations are given and the modeling results are discussed. The conclusions to the research are drawn in chapter 5. All the references used during the course of the research are listed at the end of the thesis.

CHAPTER 2

HEAT TRANSFER AT WATER-ICE INTERFACE

2.1 Ice Cover Decay

The thermal effluent discharged into the river has the most dominant effect on ice cover melting. Heat transfer from water to the ice cover is caused by convection. The fluid flow under ice cover is classified into the group of forced convections.

In convective heat transfer, the expression for the local heat transfer coefficient can be developed from the temperature profile and the thermal boundary layer thickness. This is similar to the expression for the local drag friction coefficient c_f which can be obtained from the velocity profile and the velocity boundary layer thickness. In the boundary layer region, the velocity and temperature distribution strongly influence the heat transfer by convection.

2.2 Thermal Boundary Layer and Heat Transfer Coefficient

2.2.1 Temperature Profile in the Boundary Layer

The thermal boundary layer is to profile the temperature distribution in the fluid near a solid surface. Consider a water at a uniform temperature

T_w flowing under an ice cover maintained at a constant temperature T_s, as shown in Fig. 2.1. In this figure, $\theta_\infty(x,y)$ is the dimensionless temperature profile outside the boundary layer, while $\theta_t(x,y)$ is the dimensionless temperature profile in the boundary layer which can be defined as (Ozisik, 1985):

$$\theta_t(x,y) = \frac{T(x,y) - T_s}{T_w - T_s} \tag{2.1}$$

where $\theta_t(x,y)$ = dimensionless temperature profile in the boundary layer; $T(x,y)$ = local temperature in the water; T_s = ice surface temperature; T_w = mean bulk water temperature; x, y = longitudinal and transverse directions respectively.

At the ice surface, the water temperature is equal to the ice surface temperature, hence

$$\theta_t(x,y) = 0 \quad \text{at} \quad y = 0$$

At distance sufficiently far from the ice surface, the local water temperature $T(x,y)$ is assumed to remain the same as T_w; then

$$\theta_t(x,y) \rightarrow \theta_\infty = 1$$

In the thermal boundary layer, the shape of the dimensionless temperature profile changes in both the longitudinal and transverse directions.

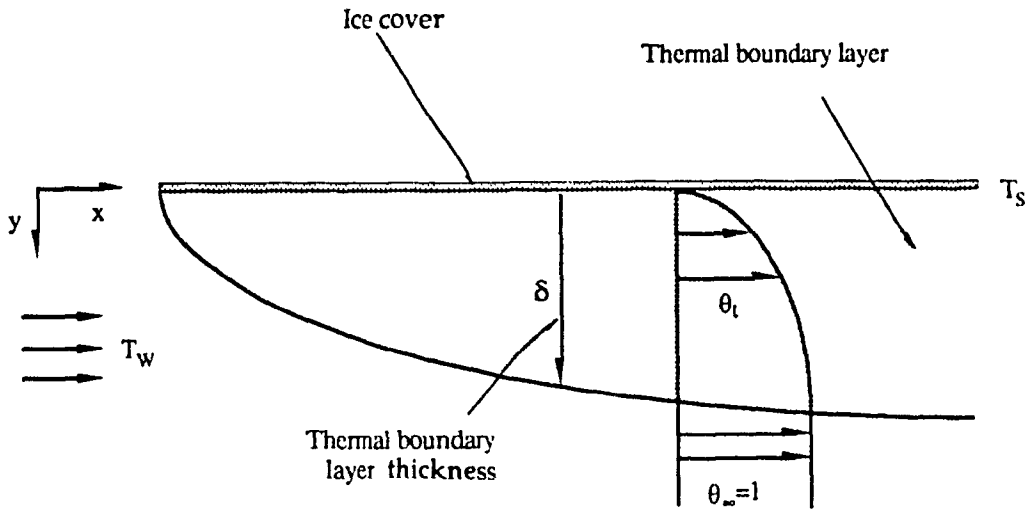

Fig. 2.1 Thermal boundary layer under an ice cover

2.2.2 Characteristics of Heat Transfer Coefficient

In a given convective heat transfer problem, the heat transfer coefficient can vary with many parameters, such as flow velocity, body shape and size, surface roughness, surface and flow temperature, and fluid properties. Nusselt Nu number is usually a function of these parameters (White, 1984):

$$Nu = f(Re, Pr, \text{generic shape}) \tag{2.2}$$

where Re = Reynolds number; Pr = Prandtl number. While the dimensionless form of the heat transfer coefficient can be expressed in terms of the Nusselt number Nu (Marsh et al., 1987):

$$Nu = \frac{h_{wi} R}{k} \tag{2.3}$$

where h_{wi} = heat transfer coefficient from water to the ice cover; k = 0.54, thermal conductivity of the water; R = hydraulic radius. In the case of ice-covered river, the hydraulic radius R is calculated as the half of the water depth (Marsh et al., 1987).

For a given fluid the Nusselt number depends primarily on the flow conditions, which can be characterized by the Reynolds number Re expressed as (Kreith, 1961):

$$Re = \frac{\rho u R}{\mu} \tag{2.4}$$

where ρ = 1000, density of water; u = velocity of the water flow; μ = dynamic viscosity of water.

In the laminar flow, the Reynolds number remains small, yielding a small heat transfer coefficient. In the turbulent flow, the heat is transferred very rapidly between the edge of the boundary layer and turbulent bulk of the flow. So large Reynolds number produces a large heat transfer coefficient.

On the other hand, the Prandtl number Pr is a function of the fluid properties alone which relates the temperature distribution to the velocity distribution. It has been defined as the ratio of the kinematic viscosity υ of the fluid to the thermal diffusivity ε of the fluid (Kreith, 1961):

$$Pr = \frac{\nu}{\varepsilon} = \frac{c_p \mu}{k} \tag{2.5}$$

where c_p = 4.1868, specific heat of water; υ = kinematic viscosity of water.

For river ice heat transfer, the heat flux (q_{wi}) from the water to the bottom surface of an ice cover can be determined by (Ozisik, 1985)

$$q_{wi}(x) = \left[- k \frac{\partial T(x, y)}{\partial y} \right]_{y = 0} \tag{2.6}$$

In terms of the local heat transfer coefficient $h_{wi}(x)$, the heat flux (q_{wi}) is given by (Ozisik, 1985)

$$q_{wi}(x) = h_{wi}(x)\,[\,T_w(x) - T_s(x)\,] \tag{2.7}$$

where x = space coordinate longitudinal direction; y = space coordinate traverse direction; $q_{wi}(x)$ = heat flux from water to the ice surface at location x along the ice cover; $h_{wi}(x)$ = heat transfer coefficient at water-ice interface at location x; $T_w(x)$ = bulk mean water temperature at location x; $T_s(x)$ = ice surface temperature at location x.

Combining Eq. (2.6) and (2.7) we obtain

$$h_{wi}(x) = \left[- \frac{k}{T_w(x) - T_s(x)} \frac{\partial T(x, y)}{\partial y} \right]_{y=0} \tag{2.8}$$

Combining Eq. (2.1) and Eq. (2.8), the local heat transfer coefficient can be expressed in terms of the dimensionless temperature profile $\theta_t(x,y)$

$$h_{wi}(x) = \left[- k \frac{\partial \theta_t(x, y)}{\partial y} \right]_{y=0} \tag{2.9}$$

As can be seen from the above Eq. (2.9) the heat transfer coefficient in the thermal entry region is a function of distance in the flow direction. In the case of ice cover melting, the dimensionless temperature profile ($\theta_t(x,y)$) along the ice cover is decreasing, which implies that in the thermal entry region the heat transfer coefficient decrease along the ice cover downstream. Eq. (2.9) is valid for heat transfer under conditions of constant surface heat flux or constant surface temperature in the thermal developing region.

The effects of the thermal entry region on the heat transfer coefficient are substantial. In this region, the heat transfer coefficient varies considerably, being the largest near the entrance and decreasing with the distance until both the velocity and the temperature profiles for a fully developed flow have been established. The thermal entry length depends on the geometry of the entrance, the roughness of the surface, and the Reynolds and the Prandtl numbers. For any given Reynolds or Prandtl number in turbulent flow, the local Nusselt number in the entrance tends to approach an asymptotic value within the length of 40 times hydraulic diameter (White, 1984). In the present modeling of ice cover melting, the entrance influence length is about 8 meters long. While the ice cover, of about 8.2 meters in length, is just within the effective influence of the thermal entrance region in the case of experimental investigation (Hewlett, 1976). The heat transfer coefficient therefore is changing with the distance in the longitudinal direction along the ice cover.

2.3 Analogy Between Heat and Momentum Transfer

2.3.1 Evaluation of Heat Transfer Coefficient

There are some methods available for the evaluation of the heat transfer coefficients in the literature. Although in most cases of practical problems, determining the heat transfer coefficient by analysis is quite difficult and impractical with available methods or by experimental investigation, a number of empirical equations for predicting heat transfer coefficient as well as the theoretical analyses for evaluating the Nusselt number have been developed. The most commonly used correlations

relating the Nusselt number Nu and Reynolds number Re to heat flux are described as below.

Colburn Equation

The Colburn equation for turbulent flow over a smooth surface in an ice covered river is expressed as (Ozisik, 1985):

$$Nu = 0.023\, Re^{0.8}\, Pr^{1/3} \tag{2.10}$$

for

$$0.7 < Pr < 160$$

$$Re > 10{,}000$$

Equation (2.10) is only applicable for the smooth surface. To account for the rough surface effect on the heat transfer coefficient, a roughness term is introduced and the Nusselt number Nu can be expressed in terms of the Manning's roughness such as (Marsh & Prowse, 1986):

$$Nu = Re\, Pr^{1/3} \frac{g\, n_i^2}{K_m^2\, R^{1/3}} \tag{2.11}$$

where n_i = Manning's roughness coefficient of ice surface; K_m = the Manning's unit conversion factor; for the ice covered river, the flow is divided into two sections. It is more accurate to use the depth of the point of

maximum velocity below the ice cover (D_o) for the hydraulic radius R (Wankiewicz, 1984):

$$D_o = \frac{D_t}{1 + (n_b / n_i)^{3/2}} \tag{2.12}$$

where D_o = depth of the point of maximum velocity below the ice cover; D_t = total flow depth; n_b = Manning's roughness coefficient of river bed. Therefore, the Nusselt number in Eq. (2.11) can be written as:

$$Nu = Re\, Pr^{1/3} \frac{g\, n_i^2 [\, 1 + (n_b / n_i)^{3/2} \,]^{1/3}}{K_m^2\, D_t^{1/3}} \tag{2.13}$$

and the heat transfer coefficient can be calculated using

$$h_{wi} = \frac{g\, n_i^2\, \rho\, c_p\, u [\, 1 + (n_b / n_i)^{3/2} \,]^{1/3}}{K_m^2\, Pr^{2/3}\, D_t^{1/3}} \tag{2.14}$$

Dittus-Boelter Equation

In the Dittus-Boelter analogy, the Nusselt number Nu is stated as (Ozisik, 1985):

$$Nu = 0.023\, Re^{0.8}\, Pr^m \tag{2.15}$$

therefore, the heat transfer coefficient can be obtained by :

$$h_{wn} = \frac{0.023\ k\ Re^{0.8}\ Pr^{m}}{R} \tag{2.16}$$

where m = 0.4 for heating and m = 0.3 for cooling of the fluid. In the case of ice cover melting, m = 0.3. The range of applicability of Eq. (2.15) is the same as for the Colburn equation. Also it only applies to the smooth surface.

Petukhov-Popov Equation

An accurate correlation, which is applicable for rough surface, has been developed by Petukhov-Popov (1963):

$$Nu = \frac{Re\ Pr}{X} \left(\frac{c_f}{2}\right) \left(\frac{\mu_b}{\mu_w}\right)^m \tag{2.17}$$

The heat transfer coefficient is given in the form

$$h_{wi} = \frac{k}{D} \frac{Re\ Pr}{X} \left(\frac{c_f}{2}\right) \left(\frac{\mu_b}{\mu_w}\right)^m \tag{2.18}$$

where

$$X = 1.07 + 12.7\ (Pr^{\frac{2}{3}} - 1)\ \left(\frac{c_f}{2}\right)^{\frac{1}{2}}$$

$$c_f = \frac{f}{4}$$

and D = hydraulic diameter; m = 0.11 for heating with uniform wall temperature; m = 0.25 for cooling with uniform solid surface temperature; m = 0 for uniform solid surface heat flux; μ_b and μ_W = viscosity at bulk fluid and

at surface respectively; c_f = drag friction factor; f = Darcy-Weisbach friction factor. Eq. (2.18) is applicable for fully developed turbulent flow in the range

$10^4 < Re < 5 \times 10^6$

$0.5 < Pr < 200$ with 5 to 6 percent error

$0.5 < Pr < 2000$ with 10 percent error

2.3.2 New Formula for Thermal Entry Region

Previous discussions of the heat transfer coefficient in turbulent flow is limited to the region where the asymptotic value of the heat transfer coefficient is reached. A practical correlation for the heat transfer coefficient at water-ice interface in the entry region of the ice cover is to be made. The heat flux is much higher in the entry region of the ice cover and a constant heat transfer coefficient is not adequate to be used in the thermal entry region of the ice cover. An equation for a variable heat transfer coefficient should be developed and applied if accurate modeling of the ice cover melting is to be achieved. The analogy between heat and momentum transfer can be utilized to derive a new correlation for the heat transfer coefficient. Such correlation should be a function of distance from the leading edge, therefore, reflecting the influence of the thermal and velocity boundary layers in this region.

When a fluid flows under an ice cover, the flow field is separated into two distinct regions. (1) The boundary layer region, in which the longitudinal velocity component varies rapidly with the distance from the ice cover and the velocity gradients and the shear stress are considered large. (2) In the

region outside the boundary layer, the velocity gradients and shear stresses are negligible, as illustrated in Fig. 2.2.

In two-dimensional flow the shearing stress τ in the boundary layer is expressed as:

$$\tau = \mu \frac{du}{dy} \tag{2.19}$$

and the rate of heat flow per unit area across an ice cover perpendicular to the y direction is

$$\frac{q_{wi}}{A} = - k \frac{dT}{dy} \tag{2.20}$$

where T = water temperature; A = area of the ice cover; q_{wi} = heat flux from water to the ice cover; k = thermal conductivity of water. Combining Eqs. (2.19) and (2.20) yields

$$\frac{q_{wi}}{A} = - \tau \frac{k}{\mu} \frac{dT}{du} \tag{2.21}$$

since $c_p = k / \mu$ (i.e., for Pr = 1) we get the equation

$$\frac{q_{wi}}{A \tau c_p} du = - dT \tag{2.22}$$

where c_p = specific heat of water. Integrating Eq. (2.22) between the limits u = 0 where $T = T_S$, and $u = u_\infty$ where $T = T_W$, yields

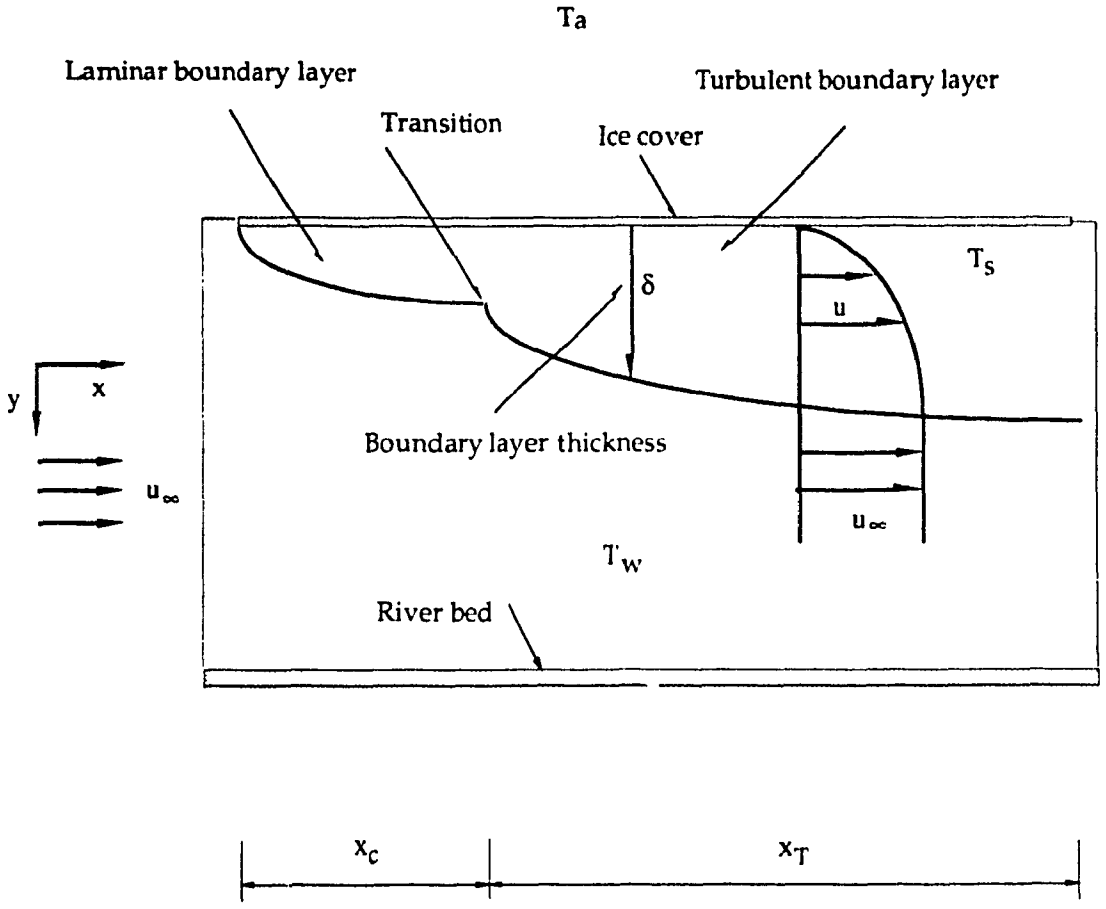

Fig. 2.2 Velocity boundary layer under an ice cover

$$\frac{q_{wi}}{A\,\tau\,c_p}\,u_\infty = (T_s - T_w) \tag{2.23}$$

where u_∞ = bulk velocity of the water. Now by definition, we have

$$h_{wi} = \frac{q_{wi}}{A\,(T_s - T_w)} \tag{2.24}$$

$$\tau = c_f \frac{\rho u_\infty^2}{2} \tag{2.25}$$

$$St = \frac{Nu}{Re\,Pr} \tag{2.26}$$

Eq. (2.26) can be given by

$$St = \frac{Nu}{Re\,Pr} = \frac{h_{wi}}{\rho\,c_p u_\infty} = \frac{c_f}{2} \tag{2.27}$$

where c_f = drag friction factor; St = Stanton number.

Eq. (2.27) is known as the Reynolds analogy for momentum and heat transfer in fully developed turbulent flow over a flat surface which relates the Stanton number St, or heat transfer coefficient, to the drag friction factor c_f. However, it is only valid for Prandtl number Pr = 1.

On the basis of the Reynolds analogy, Colburn developed a modified analogy based on experimental investigations. He found that correlating heat

transfer data for fluids having Prandtl numbers ranging from 0.6 to about 50 requires the correction of Stanton number in Eq. (2.27) by a factor of $Pr^{2/3}$, or (Colburn, 1933)

$$St\, Pr^{2/3} = \frac{c_f}{2} \tag{2.28}$$

This expression is referred to as the Colburn analogy which can apply to laminar as well as turbulent flow under an ice cover.

To apply this analogy in practice it is necessary to know the friction factor c_f. In view of the flow behaviors, the friction forces are also governed by the boundary layer characteristics, which is large near the leading edge of the surface and decreases with increasing distance from the leading edge. One of the empirical equations, used to evaluate the local friction factor for a turbulent flow over a flat smooth surface with Reynolds number range between 5×10^5 and 10^7, is given by (Kreith, 1961):

$$c_f = 0.0576 \left(\frac{u_\infty x_L}{\upsilon}\right)^{1/5} \tag{2.29}$$

where x_L = distance from the leading edge of the flat surface; υ = kinematic viscosity of the water.

This equation is valid for fully developed turbulent boundary layer and confined to a smooth surface. The value of c_f given by this equation is much

smaller than those corresponding to a rough surface particularly in the entry region. It is therefore necessary to introduce the roughness effects into this equation. In fact, the effects of the roughness as well as of the entry region can be combined to be reflected by a single factor, the friction factor or the roughness coefficient in the entrance region of the ice cover.

In reality the boundary layer under an ice cover generally begins with laminar flow over the forward portion of the ice cover and becomes turbulent layer beyond, as illustrated in Fig. 2.2. The occurrence of the transition from the laminar boundary layer to turbulent boundary layer depends on the Reynolds number, which is usually in the range of 5×10^5 and 10^7 (Kreith, 1961). However, this critical value is strongly dependent on the surface roughness as well as the geometry of the fluid. With very large disturbance, the transition may begin at a Reynolds number lower than that value. In the present study, because of the presence of the ice cover on the channel flow with its rough surface of the underside and blunt edge of the ice cover, it is, therefore, reasonable to assume that the turbulent boundary layer starts at the beginning of the ice cover ($x_c = 0$). Therefore, the average friction coefficient over the surface of the ice cover with length L can be obtained by integrating Eq. (2.29), or

$$\bar{c}_f = \frac{1}{L}\int_0^L c_f \, dx = 0.072 \left(\frac{u_\infty L}{\upsilon}\right)^{-1/5} \tag{2.30}$$

and by definition we have (Henderson, 1966)

$$\frac{f}{8} = \frac{c_f}{2} \tag{2.31}$$

$$f = \frac{8\, g\, n_m^2}{R^{1/3}} \tag{2.32}$$

where f = Darcy-Weisbach friction factor. Combining Eqs. (2.30), (2.31) and (2.32) we get the following expression for mean Manning's roughness coefficient corresponding to a smooth surface of an ice cover:

$$n_m^2 = \frac{0.072}{2\, g} R^{1/3} \left(\frac{u_\infty L}{\nu}\right)^{-1/5} \tag{2.33}$$

where L = total length of an ice cover; n_m = mean Manning's coefficient over an ice cover.

Mean Manning's coefficient n_m obtained from Eq. (2.33) is only valid for a smooth surface. A correlation factor c_n is introduced to the friction factor in accordance with the roughness coefficient of a rough surface in the entry region:

$$c_n = \frac{n_{ie}^2}{n_m^2} \tag{2.34}$$

and Eq. (2.29) becomes

$$c_{fn} = 0.0576\, c_n \left(\frac{u_\infty x_L}{\upsilon}\right)^{-1/5} \tag{2.35}$$

where n_{ie} = Manning's roughness coefficient over the ice cover; c_n = friction correlation factor; c_{fn} = friction factor for rough surface.

Therefore, a new approach for predicting the heat transfer coefficient for the ice cover particularly suitable for the entry region is then developed by combining Eqs. (2.35) and (2.27):

$$h_x = 0.0288\, c_n \frac{k}{x_L^{0.2}} Pr^{1/3} \left(\frac{u_\infty}{\upsilon}\right)^{0.8} \tag{2.36}$$

where h_x = local heat transfer coefficient.

It can be seen from the equation (2.36) that the value of the heat transfer coefficient is proportional to $1/x^{0.2}$, indicating that the heat flux obtained by using Eq. (2.36) is decreasing with the distance, or being large in the entrance and decreasing toward an asymptotic value. The equation can apply to the entry region or the short length of the ice cover for either smooth or rough surface as long as the friction factor is properly correlated.

CHAPTER 3

TWO-DIMENSIONAL NUMERICAL MODEL

3.1 Introduction

A two-dimensional numerical model was utilized in the present work to predict ice cover melting using different heat transfer coefficients. Three empirical formulas, the Dittus-Boelter, the Colburn, and the Petukhov-Popov equations, together with the proposed correlation, were used to compute the heat transfer coefficient at ice-water interface. These equations were computed at each computational time step during the modeling process to produce the corresponding instantaneously values of the heat transfer coefficient. Results generated from the modeling have been compared with experimental and field data.

3.2 Governing Equations

3.2.1 Hydrodynamic Equations

The river hydrodynamics field is established by using the depth integrated St. Venant shallow water equations, which express the principles of conservation of mass and momentum in x and y directions respectively:

Continuity equation:

$$\frac{\partial h}{\partial t} + \frac{\partial uh}{\partial x} + \frac{\partial vh}{\partial y} = 0 \tag{3.1}$$

Conservation of momentum equation in x direction:

$$\frac{\partial U}{\partial t} + \frac{\partial E}{\partial x} + \frac{\partial F}{\partial y} = g\,h\frac{\partial \Gamma}{\partial x} + \frac{\partial}{\partial x}\left(\frac{\tau_{xx}}{\rho}\right) + \frac{\partial}{\partial y}\left(\frac{\tau_{xy}}{\rho}\right) + \frac{\tau_{sx}}{\rho} - \frac{\tau_{bx}}{\rho} \tag{3.2}$$

Conservation of momentum equation in y direction:

$$\frac{\partial V}{\partial t} + \frac{\partial F}{\partial x} + \frac{\partial G}{\partial y} = g\,h\frac{\partial \Gamma}{\partial y} + \frac{\partial}{\partial x}\left(\frac{\tau_{yx}}{\rho}\right) + \frac{\partial}{\partial y}\left(\frac{\tau_{yy}}{\rho}\right) + \frac{\tau_{sy}}{\rho} - \frac{\tau_{by}}{\rho} \tag{3.3}$$

where the conservative variables E, F, G and Γ are defined as:

$$E = E(x,y,t) = u^2 h \tag{3.4}$$

$$F = F(x,y,t) = u\,v\,h \tag{3.5}$$

$$G = G(x,y,t) = v^2 h \tag{3.6}$$

$$\Gamma = H + 0.92\,\theta \tag{3.7}$$

and τ_{bx} and τ_{by} = bottom stresses in the x and y directions respectively given by equations (3.8) and (3.9):

$$\frac{\tau_{bx}}{\rho} = g\, h\, S_{fx} \tag{3.8}$$

$$\frac{\tau_{by}}{\rho} = g\, h\, S_{fy} \tag{3.9}$$

where S_{fx}, S_{fy} = friction slopes expressed as

$$S_{fx} = \frac{n^2\, u \sqrt{(u^2 + v^2)}}{R^{4/3}} \tag{3.10}$$

$$S_{fy} = \frac{n^2\, v \sqrt{(u^2 + v^2)}}{R^{4/3}} \tag{3.11}$$

τ_{xx}, τ_{xy} (= τ_{yx}) and τ_{yy} are depth averaged turbulent stresses expressed as:

$$\frac{\tau_{xx}}{\rho} = \nu_t \left(2 \frac{\partial uh}{\partial x}\right) \tag{3.12}$$

$$\frac{\tau_{xy}}{\rho} = \nu_t \left(\frac{\partial uh}{\partial y} + \frac{\partial vh}{\partial x}\right) \tag{3.13}$$

$$\frac{\tau_{yy}}{\rho} = \nu_t \left(2 \frac{\partial vh}{\partial y}\right) \tag{3.14}$$

In all equations above, x and y = planer coordinates; t = time; H = h + Z_f; Z_f = bed elevation; h = h(x,y,t) local water depth; U = U(x,y,t) = uh and V = V(x,y,t) = vh unit width discharges in x and y directions respectively; θ = ice cover thickness; ν_t = turbulent viscosity; κ = turbulent kinetic energy. τ_{sx} and τ_{sy} = surface stresses; ρ = water density which is assumed constant. The value of 92% is employed to account for the density ratio between ice and water. R = hydraulic radius; n = combined Manning's roughness coefficient of ice and river bed. In the case of open water the hydraulic radius is set equal to the water depth. But for an ice covered flow the hydraulic radius is equal to one half the river depth. For the open water flow the Manning's coefficient is determined by bed friction. For an ice covered river a combined Manning's coefficient for river bed and ice cover underside is from Sabeneev formula (Wankiewicz, 1984):

$$n = \left(\frac{n_b^{3/2} + n_i^{3/2}}{2} \right)^{2/3} \tag{3.15}$$

where n_b and n_i = Manning's coefficients of river bed and ice cover underside respectively.

3.2.2 Energy Equation

The temperature distribution in the river flow field is calculated by the use of the two-dimensional unsteady heat energy conservation equation governing the temperature distribution in a vertically homogeneous stream which is given by:

$$\frac{\partial Th}{\partial t} + \frac{\partial TU}{\partial x} + \frac{\partial TV}{\partial y} = \frac{\partial}{\partial x}(h D_x \frac{\partial T}{\partial x}) + \frac{\partial}{\partial y}(h D_y \frac{\partial T}{\partial y}) + h \Phi \qquad (3.16)$$

where T = water temperature; Φ = source term which represents the heat flux from water to atmosphere; D_x, D_y = longitudinal dispersion coefficients in the x- and y-directions respectively given as (Ashton, 1979)

$$D_x = k_x U^* R \qquad (3.17)$$

$$D_y = k_y V^* R \qquad (3.18)$$

where k_x, k_y = dispersion constants in the x- and y- directions respectively; U^*, V^* = shear velocities in x- and y- directions respectively and are defined as

$$U^* = \sqrt{S_{fx} g R} \qquad (3.19)$$

$$V^* = \sqrt{S_{fy} g R} \qquad (3.20)$$

3.3 Heat Transfer Equations

3.3.1 Top Surface Heat Exchange

The phenomena of top ice melting is the result of the heat transfer at air-ice interface. When the river is not ice covered heat transfer occurs at air-

water interface. Each individual heat exchange process is influenced by the river surface conditions.

The surface heat exchange process consists of following major components: (1) solar (shortwave) radiation, ϕ_{ri}; (2) long-wave radiation, ϕ_b; (3) evaporative heat flux, ϕ_e; (4) convective heat transfer, ϕ_c. However, the heat transfer from precipitation and geothermal heat transfer through the river or channel bed are not significant in modeling the ice melting. The meteorological conditions influencing these components are cloud cover, air temperature, wind velocity and air vapor pressure.

The heat transfer due to these processes are shown schematically in Fig. 3.1.

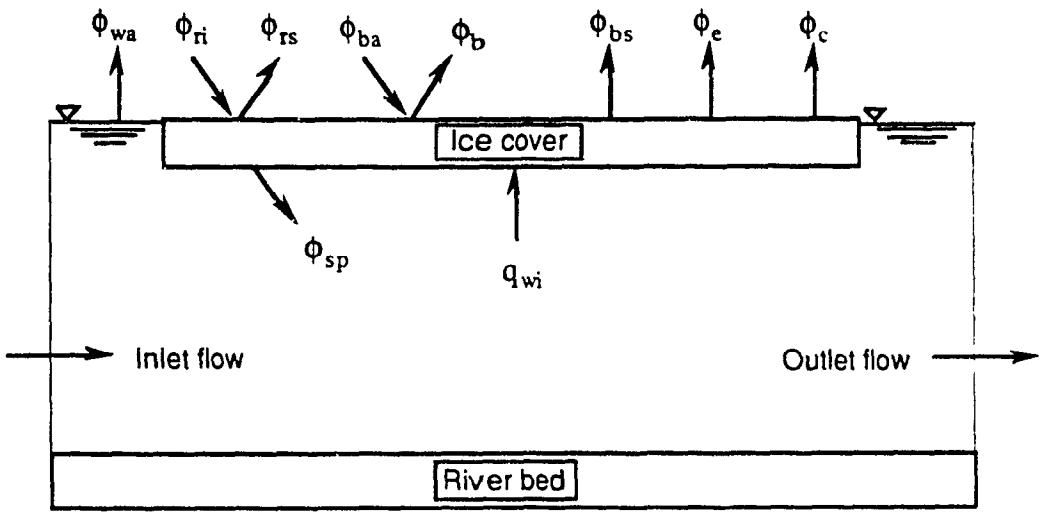

Fig. 3.1 Heat transfer at air-ice, water-ice and air-water interfaces

Short-Wave Radiation

The solar radiation outside the earth's atmosphere varies with distance from the sun which may be determined from weather records on cloud cover conditions. A part of the solar radiation is reflected, while the another part reaches the ground surface. When clouds are present, most of the radiation will scatter and be absorbed. Under heavy clouds all radiation reaching the ground surface will be diffuse. The incoming solar radiation can be therefore calculated using the cloud cover data such as (Shen & Chiang, 1984)

$$\phi_{ri} = \left(a - b\,(\phi_{lat} - 50)\right)(1 - 0.0065\,C^2) \qquad (3.21)$$

where ϕ_{ri} = incoming shortwave radiation; ϕ_{lat} = latitude on the earth's surface; C = cloud cover in tenths (ranging from 0 for a clear sky to 10 for a completely overcast sky). The constants a and b reflect the annual variation in solar radiation intensity, which are given in Table 3.1 for the winter period (Shen & Chiang, 1984).

Table 3.1 Annual Variation of Solar Radiation Constants (Shen & Chiang, 1984)

Month	a	b
December	418	8.2
January	595	11.0
February	955	11.2
March	1650	12.7
April	2319	8.4

Since part of the solar radiation reaching the water surface is reflected back into the atmosphere, the net solar radiation for the water surface is in the form

$$\phi_s = (1 - \alpha) \phi_n \tag{3.22}$$

where ϕ_s = net shortwave radiation; α = 0.1, surface albedo.

In the case of the ice cover, the value of albedo is determined from the material behavior of the ice cover. The albedo is obtained from (Shen & Chiang, 1984)

$$\alpha = \alpha_i \qquad T_a \leq 0\ ^{o}C \tag{3.23}$$

$$\alpha = \alpha_a + (\alpha_i - \alpha_a) e^{-\psi T_a} \qquad T_a \geq 0\ ^{o}C \tag{3.24}$$

where α_i, α_a, and ψ = empirical constants, their values are 0.41, 0.25, 0.7, respectively; T_a = air temperature.

A portion of solar radiation penetrating the ice cover can be considered as an internal heat source in the water body. The penetration of the shortwave radiation is calculated from:

$$\phi_{sp} = \beta_i \phi_s e^{-\tau_i \theta} \tag{3.25}$$

where ϕ_{sp} = penetration of the shortwave radiation into the water body; β_i = fraction of absorbed solar radiation which penetrates the ice-water interface; τ_i = 0.07, bulk extinction coefficient. The value of β_i is chosen as 1.0 due to the small difference in the refractive indices of ice and water.

Long-wave Radiation

The long-wave radiation is influenced by the meteorological factors and it consists of two components. These components are the long-wave radiation emitted from the river surface and the net absorbed atmospheric radiation.

According to the Stefan-Boltzmann law the radiation emission from the river surface is predicted from (Shen & Chiang, 1984)

$$\phi_{bs} = \varepsilon_s \sigma T_{sk}^4 \tag{3.26}$$

where ϕ_{bs} = long-wave radiation emitted by the river surface; ε_s = 0.97, emissivity of both the water and ice surface; σ = 4.903 x 10^{-7}, Stefan-Boltzmann constant; T_{sk} = water or ice surface temperature.

The atmospheric radiation is generally expressed as a function of air temperature which can be obtained from weather records. Under clear skies the atmospheric radiation can be computed from:

$$\phi_{ba} = \sigma T_{ak}^4 (c + d \sqrt{e_a}) \tag{3.27}$$

and for the cloudy condition, the correlation of the radiation is using Bolz's formula (Shen & Chiang, 1984)

$$\phi_{ba} = \sigma T_{ak}^4 (c + d \sqrt{e_a}) (1 + k_c C^2) \tag{3.28}$$

where ϕ_{ba} = atmospheric radiation; T_{ak} = air temperature; e_a = air vapor pressure; c, d, k_c = empirical constants, their values are 0.55, 0.052 and 0.0017, respectively.

With emittances of 0.97 for water or ice cover, the net radiation can be finally calculated as

$$\phi_b = \phi_{bs} - 0.97 \phi_{ba} \tag{3.29}$$

where ϕ_b = net radiation.

Evaporative Heat Flux

Evaporative heat transfer from water surface can be calculated by the Rimsha-Donchenko formula (Shen & Chiang, 1984)

$$\phi_e = \left(1.56 \left[8.0 + 0.35 \left(T_{ws} - T_a \right) \right] + 6.08\, V_a\right) \left(e_s - e_a \right) \qquad (3.30)$$

where ϕ_e = evaporative heat flux; V_a = wind velocity; e_s = saturation vapor pressure at the water surface temperature; T_{ws} = water surface temperature.

When an ice cover is present, the value of 0.5 is added to Eq. (3.30) due to reduction in the evaporative process:

$$\phi_e = 0.5 \left(1.56 \left[8.0 + 0.35 \left(T_{ws} - T_a \right) \right] + 6.08\, V_a\right) \left(e_s - e_a \right) \qquad (3.31)$$

Convective Heat Flux

The convective heat flux is calculated using the Rimsha-Donchenko formula (Shen & Chiang, 1984)

$$\phi_c = C_c \left(8.0 + 0.35 \left(T_s - T_a \right) + 3.9\, V_a\right) \left(T_s - T_a \right) \qquad (3.32)$$

where C_c = 0.5, coefficient accounting for the reduction in convective heat transfer due to the presence of the ice cover.

Top Surface Ice Melting

The top surface temperature of the ice cover is determined by the heat exchange at the air-ice interface, which is obtained from (Shen & Chiang, 1984)

$$\phi_s (1 - \beta_i e^{-\tau_i \theta}) - \phi_b - \phi_e - \phi_c + k_i \frac{T_f - T_s}{\theta} = 0 \quad (T_s \leq 0^oC) \qquad (3.33)$$

where k_i = 2.219, thermal conductivity of ice; T_f = 0 °C, freezing point temperature for fresh water.

When the top surface temperature calculation is performed, the surface temperature may exceed (>) 0°C, the melting point of ice. In this case, the top surface temperature (Ts) is set to 0°C and the top surface melting is calculated using:

$$\phi_s (1 - \beta_i e^{-\tau_i \theta}) - \phi_b - \phi_e - \phi_c = - \rho_i L_i \frac{\Delta\theta_s}{\Delta t} \quad (T_s = 0^oC) \qquad (3.34)$$

where ρ_i = 920, density of the ice; L_i = 33.5 x 10^4 , latent heat of fusion of ice; $\Delta\theta_s$ = change in the ice thickness at the upper surface during the time step Δt.

3.3.2 Bottom Surface Heat Exchange

Heat flux from water to ice cover has the most dominant effect on the ice melting. Heat flux calculation from water to underside of the ice cover is given (Kreith, 1963)

$$q_{wi} = h_{wi} (T_w - T_s) \tag{3.35}$$

where q_{wi} = heat transfer from the water to ice cover; h_{wi} = heat transfer coefficient at water-ice interface; T_w = bulk water temperature. The formula for the calculation of heat transfer coefficient has been discussed in detail in chapter 2.

Assuming a linear temperature profile through the ice cover, the bottom surface melting is determined by (Shen & Chiang, 1984)

$$K_i \frac{T_f - T_s}{\theta} - q_{wi} = \rho_i L_i \frac{\Delta\theta_w}{\Delta t} \tag{3.36}$$

where $\Delta\theta_w$ = change in ice thickness at bottom surface during the time step Δt.

3.3.3 Source Term Calculation

The heat exchange components in the energy equation (3.16) depends on whether the river is ice covered or not. In the case of an ice cover the source term ϕ is given by (Shen & Chiang, 1984)

$$\phi = \phi_{sp} - q_{wi} \tag{3.37}$$

and for the case without an ice cover

$$\phi = \phi_s - \phi_b - \phi_e - \phi_c \tag{3.38}$$

therefore the source term can be determined from

$$\Phi = \frac{\phi}{C_p\, h\, \rho} \tag{3.39}$$

3.4 Numerical Solution

3.4.1 Hydrodynamic Equation Solution

Solution of the hydrodynamics equations (Eq. (3.1), (3.2) and (3.3)) is obtained by use of the finite difference scheme, which is an explicit, forward time central space scheme based on a modified version of the MacCormack method. A finite difference grid is overlain on the hydrodynamic field with all values defined at each grid point. In the MacCormack scheme, the two-dimensional operator is split into a sequence of one-dimensional operators. Each operator is further split into a predictor-corrector sequence described as follow:

$$L(\Delta t) = L_x(\Delta t_x)\, L_y(\Delta t_y)\, L'_y(\Delta t_y)\, L'_x(\Delta t_x) \tag{3.40}$$

where L_x, L_y = one dimensional finite difference operators, respectively; Δt_x , Δt_y = half the time increment Δt.

Therefore the solution at each time increment for each grid (i,j) is obtained by

$$W_{i,j}^{n+1} = L_x (\Delta t_x) L_y (\Delta t_y) L_y' (\Delta t_y) L_x' (\Delta t_x) W_{i,j}^n \tag{3.41}$$

where W = flow characteristic, such as velocity or water depth.

Fig. 3.2 shows the finite difference grid. Subscripts of i indicate points in the x direction and j indicate points in the y direction. The MacCormack operator, in x direction applied to the hydrodynamic equations yields (Garcia, 1983)

$$h_{i,j}^{n+1/2} = h_{i,j}^n - \frac{\Delta t_2}{\Delta x} (U_{i,j}^n - U_{i-1,j}^n) \tag{3.42}$$

$$\begin{aligned} U_{i,j}^{n+1/2} = U_{i,j}^n - \frac{\Delta t_2}{\Delta x} (F_{i,j}^n - F_{i-1,j}^n) + g \Delta t_2 (\frac{h_{i,j}^n + h_{i-1,j}^n}{2}) \\ \left(- (\frac{Z_{fi,j} - Z_{fi-1,j}}{\Delta x}) - S_{fxi,j}^n \right) + \Delta t_2 (f V_{i,j}^n - \frac{\tau_{sxi,j}^n}{\rho}) \\ + \varepsilon \frac{\Delta t_2}{\Delta x^2} (U_{i-1,j}^n - 2 U_{i,j}^n + U_{i+1,j}^n \end{aligned} \tag{3.43}$$

$$V_{i,j}^{n+1/2} = V_{i,j}^n - \frac{\Delta t_2}{\Delta x} (G_{i,j}^n - G_{i-1,j}^n) + \varepsilon \frac{\Delta t_2}{\Delta x^2} (V_{i-1,j}^n - 2 V_{i,j}^n + V_{i+1,j}^n) \tag{3.44}$$

where Δt_2 = one half the time step Δt.

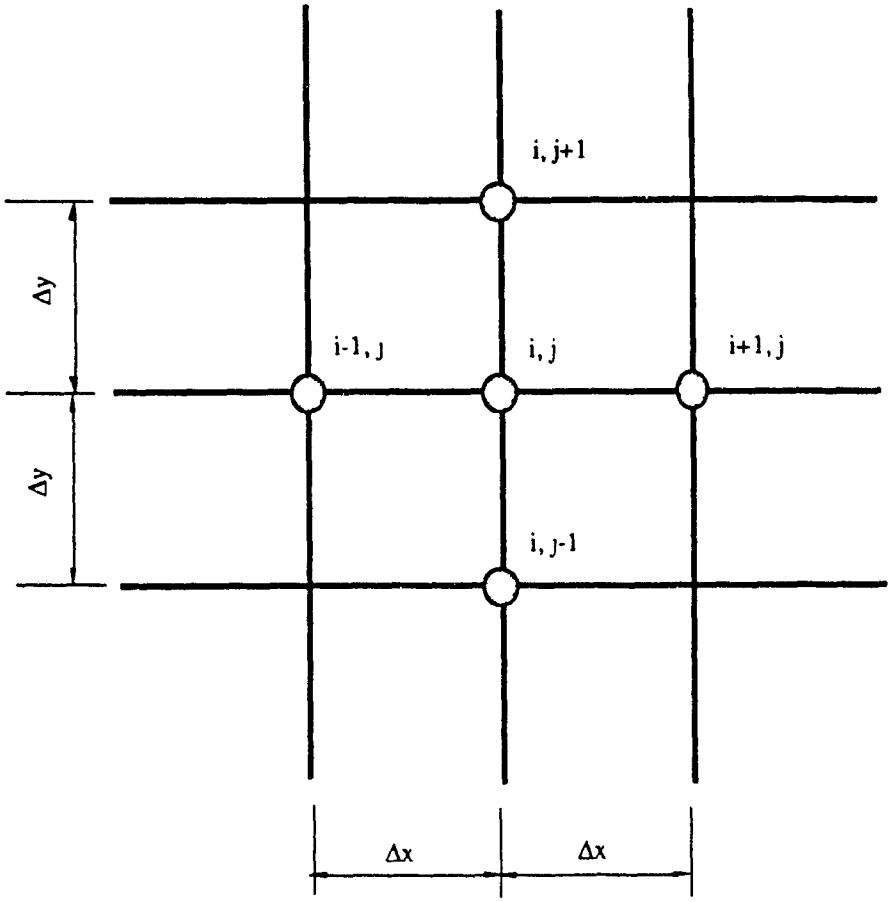

Fig. 3.2 Illustration of finite difference grid

The stability criteria for the finite difference scheme is determined by the Courant-Friedrich-Levy criterion. The maximum time step in the modified MacCormack scheme is given by (Baldwin, MacCormack & Diewart, 1975)

$$\Delta t \leq \text{Min}\left(\frac{2\,\Delta x}{u + \sqrt{g\,h}}, \frac{2\,\Delta y}{v + \sqrt{g\,h}}\right) \tag{3.45}$$

The time step chosen should be the minimum value of these two.

3.4.2 Energy Equation Approximations

The upwind scheme is employed to solve the temperature equation including convection and dispersion in the flow domain. In the upwind scheme it is assumed that the heat is transferred from the upstream of the flow to the downstream. Fluid flowing from upstream to the downstream is at the temperature that prevails on the upstream and does not know anything about the fluid toward which it is heading, but carries the full characteristic of the fluid from which it has come. The upwind scheme is illustrated in Fig. 3.3 (Patankar, 1980):

when $U > 0$ $\quad T_e = T_p,\ T_p = T_w$

when $U < 0$ $\quad T_e = T_E,\ T_p = T_e$

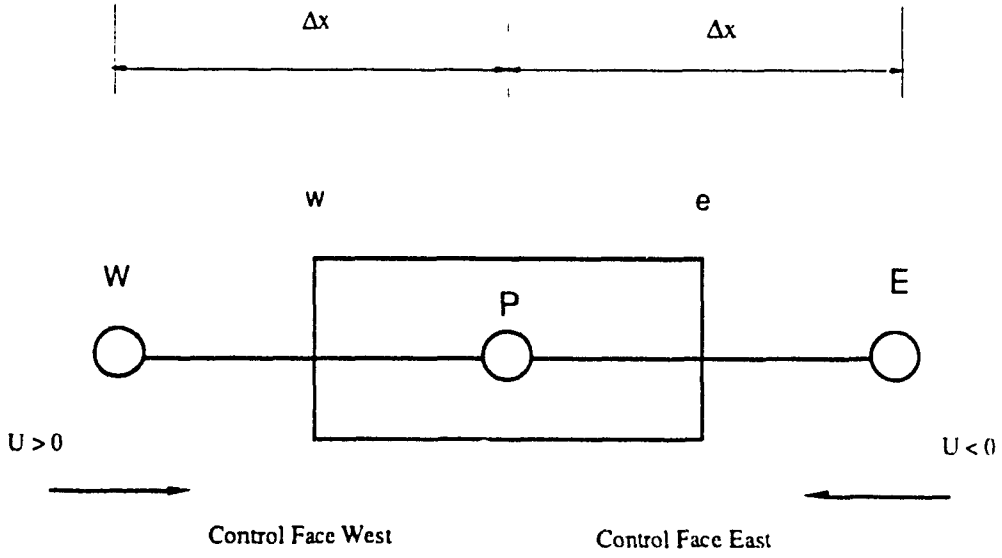

Fig. 3.3 Illustration of upwind scheme

The discritization of the two-dimensional energy equation is given by

$$h_{i,j}^{n+1}\, T_{i,j}^{n+1} = h_{i,j}^{n+1}\, T_{i,j}^{n} - \Delta t \left(\frac{\partial UT}{\partial x} + \frac{\partial VT}{\partial y} \right) +$$

$$\frac{\Delta t}{\Delta x^2} \left(D_{xi+(1/2),j}^{n+1}\, h_{i+(1/2),j}^{n+1} \left(T_{i+1,j}^{n} - T_{i,j}^{n} \right) - D_{xi-(1/2),j}^{n+1}\, h_{i-(1/2),j}^{n+1} \left(T_{i,j}^{n} - T_{i-1,j}^{n} \right) \right) +$$

$$\frac{\Delta t}{\Delta y^2} \left(D_{yi,j+(1/2)}^{n+1}\, h_{i,j+(1/2)}^{n+1} \left(T_{i,j+1}^{n} - T_{i,j}^{n} \right) - D_{yi,j-(1/2)}^{n+1}\, h_{i,j-(1/2)}^{n+1} \left(T_{i,j}^{n} - T_{i,j-1}^{n} \right) \right) +$$

$$\Delta t \left(h_{i,j}^{n+1}\, \Phi_{i,j}^{n+1} \right) \qquad (3.46)$$

where

$$\frac{\partial UT}{\partial x} = \frac{U_{i+(1/2),j}\, T_{i,j} - U_{i-(1/2),j}\, T_{i-1,j}}{\Delta x} \quad \text{for } U_{i-(1/2),j} \text{ and } U_{i+(1/2),j} > 0 \qquad (3.47)$$

$$\frac{\partial UT}{\partial x} = \frac{U_{i+(1/2),j}\, T_{i+1,j} - U_{i-(1/2),j}\, T_{i,j}}{\Delta x} \quad \text{for } U_{i-(1/2),j} \text{ and } U_{i+(1/2),j} < 0 \qquad (3.48)$$

$$U_{i-(1/2),j} = \frac{U_{i-1,j} + U_{i,j}}{2} \qquad (3.49)$$

$$U_{i+(1/2),j} = \frac{U_{i,j} + U_{i+1,j}}{2} \qquad (3.50)$$

3.4.3 Initial and Boundary Conditions

To solve the governing equations the initial and boundary conditions are needed, together with geometrical data of the area in which the solutions

are sought. The initial and boundary conditions have to fulfil certain conditions in order that the problem is well posed.

The initial and boundary conditions depend on the actual flow situation and a number of boundary values have to be prescribed to determine the solution. Table 3.2 shows the required boundary conditions for the hydrodynamic equations.

Table 3.2 Number of boundary conditions for 2-D problems

Sub-critical flow $u^2 + v^2 \leq gh$		Super-critical flow $u^2 + v^2 > gh$	
Inflow	Outflow	Inflow	Outflow
2	1	3	0

The water depth at all computational points is initially specified to the outflow boundary water depth. Temperature at all points is set to the inflow temperature. The water velocity components are initially set to zero over all computational zone. Initial ice thickness is set according to laboratory record. Fig. 3.4 shows the boundary conditions at closed boundary.

Closed boundaries are locations where solid walls limit the flow field such as river banks. The velocity perpendicular to the wall is equal to zero at all time and non slip boundary condition applies when ε is not zero. The temperatures of the fictitious point are set to the temperature of the inside adjacent cell. Convection and dispersion are zero at the boundary due to zero

wall velocity and zero temperature gradient across the boundary, resulting zero heat flux at the bank.

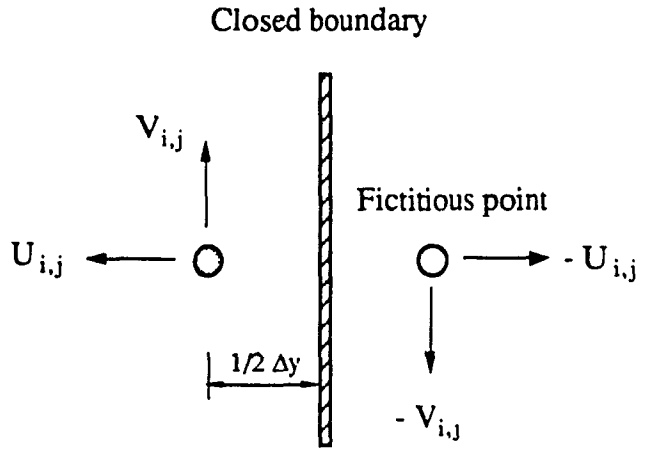

Fig. 3.4 Boundary conditions at closed boundary

CHAPTER 4

MODEL APPLICATION AND DISCUSSION

Different heat transfer coefficients employed in ice melting calculation can lead to different melting predictions. The study of the behavior of ice cover melting using a number of different heat transfer coefficients was carried out through the application of a two-dimensional numerical model. Three different empirical equations, the Dittus-Boelter and the Colburn, the Petukhov-Popov equations together with the new derived formula were applied respectively in the model to compare their effects on the ice melting. The computational results were compared to experimental observations and field study as well.

4.1 Computational Procedures

Computational procedures were performed by first solving the hydrodynamic equations, i.e. the continuity equation, momentum equations, to obtain a steady flow field before an ice cover was imposed on top of the water. Then, the thermal effluent was introduced and the solutions of the energy equation were obtained until a steady hydrothermal flow field was established. Based on the steady hydrothermal flow field the heat transfer processes between air-ice, air-water and water-ice interfaces were considered. Before conducting the computations of the heat flux between water and the ice cover surface underside, three empirical equations, for the calculation of

the heat transfer coefficient as well as the new formula, were computed at each grid point according to the hydrothermal considerations. Consequently, the model evaluates the ice cover growth and decay as a result of the heat transfer processes. Continued use of the hydrodynamic equations allowed for the consideration of variations in the flow field due to the continuous changes in the ice cover thickness.

Repetition of these steps would advance the numerical solution through any desired time level. In modelling laboratory experiments, a maximum time of 300 minutes melting was considered corresponding to the actual experimental time.

4.2 Experimental Conditions

A total of seven experiments were conducted by Hewlett at Iowa University in 1976 (Hewlett, 1976). However, data from three of these experiments were utilized in the above studies, among which experimental run 1# had complete data. Therefore, experimental run 1# conditions were simulated in the model and modeling results were compared to the corresponding data.

In the laboratory experiments, the channel had a length of 12 meters and a width of 0.6 meter as shown in Fig. 4.1. The average unit width discharge of the channel was about 0.037 m^2/s with a slight variation with time as shown in Fig. 4.2. The water depth in the channel under ice cover was about 0.2 meters and the slope of the channel was near zero to 0.025.

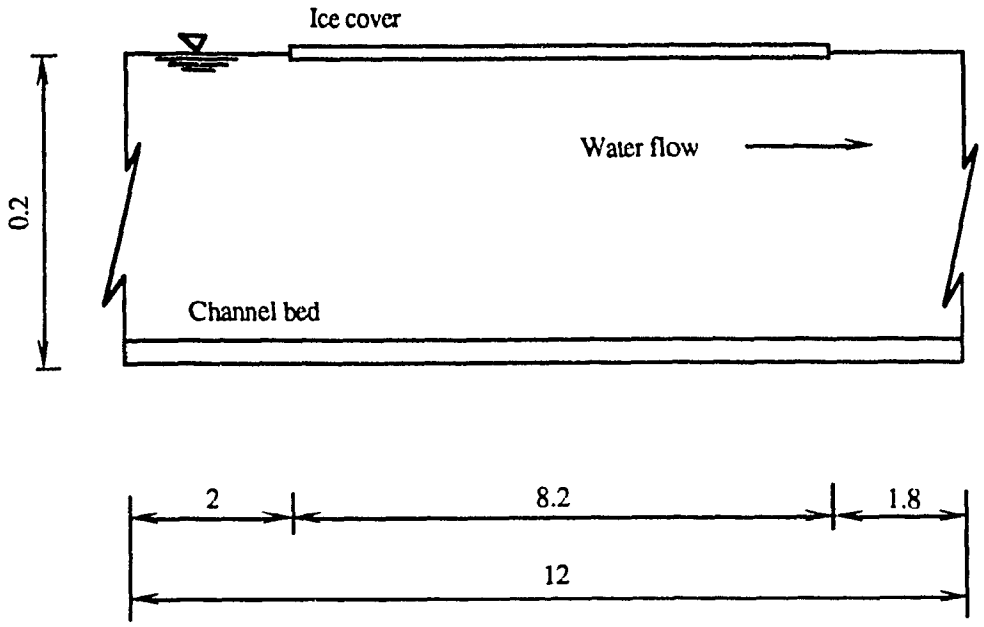

(All dimensions are in m)

Fig. 4.1 Channel geometry used in experiment 1#

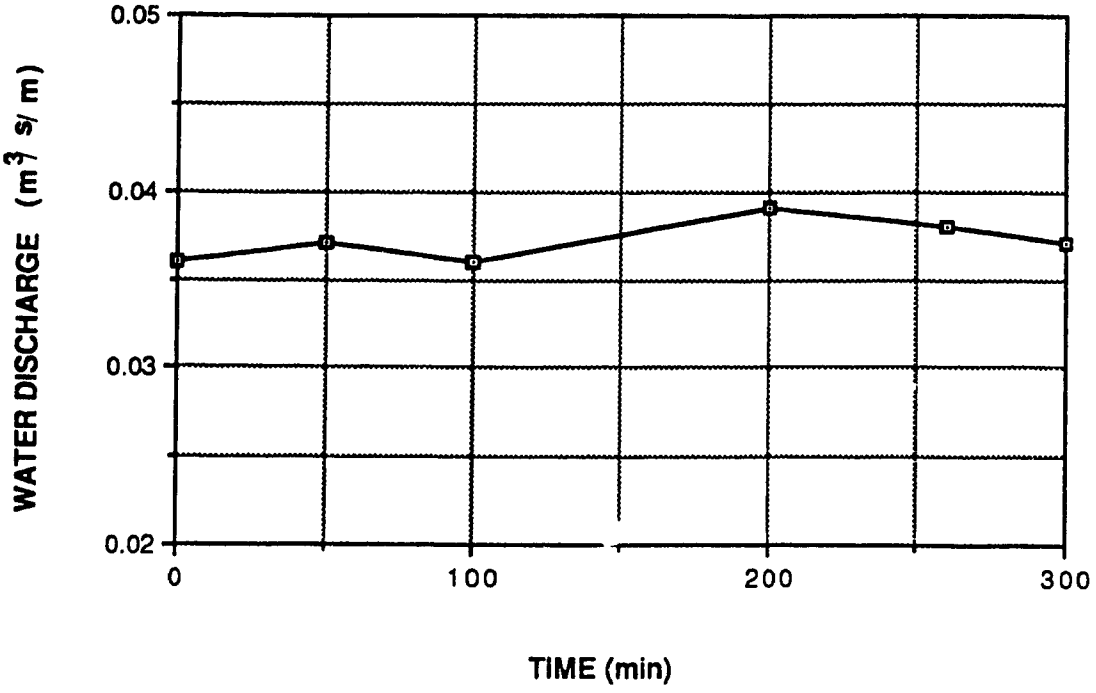

Fig. 4.2 Water discharge variation with time during experiment #1

The mean water temperature was about 1 °C and the laboratory ambient temperature was near 0 °C. The variation of inlet water temperature with time is shown in Fig. 4.3. Both the variations of the discharge and thermal effluent temperature in the inlet of the channel were accurately reproduced at each computational time step following the experimental records.

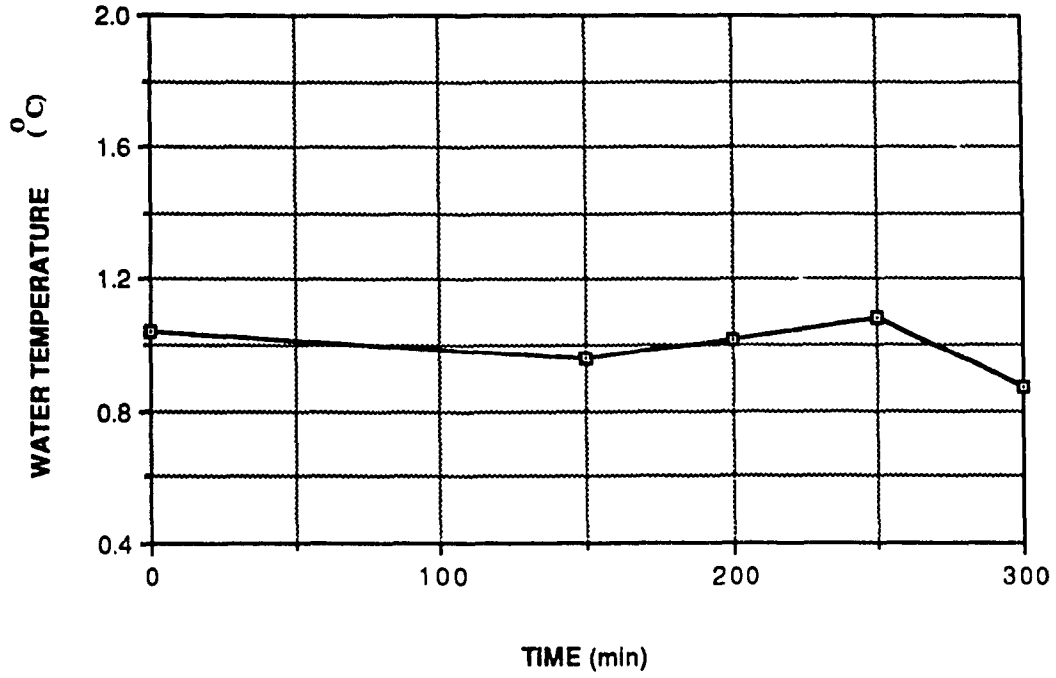

Fig. 4.3 Water temperature variation with time during experiment #1

An ice cover was formed on top of the water with a length of 8.2 meters starting at about 2 meters downstream from the channel inlet. The average initial ice cover thickness was about 0.05 meter but differed slightly from one point to another. The profile of initial ice cover thickness is shown in Fig. 4.4. The initial conditions in the model were set to the actual thickness of the ice cover as given at each point. In chapter 2 it was established that the length of thermal entrance influence is about 8 meters, which means the length of the ice cover used in the experiments was just within the effective length of thermal entrance region. The heat transfer coefficient in this region is therefore a function of distance in the flow direction and could not be taken as a constant.

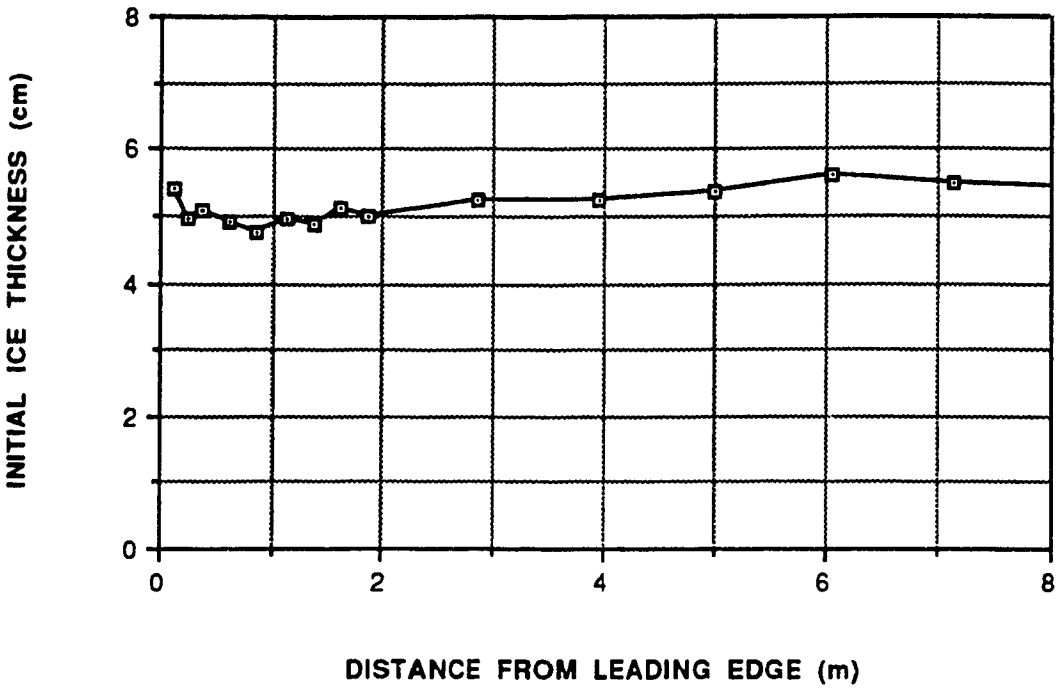

Fig. 4.4 Initial ice cover thickness in experiment #1

The probes designed to measure the ice cover thickness in experiments were installed at distances varied from 0.12 meter near the leading edge to 1.5 meter towards the downstream end of the channel as shown in Fig. 4.5. Table 4.1 lists the distance of each probe from the leading edge.

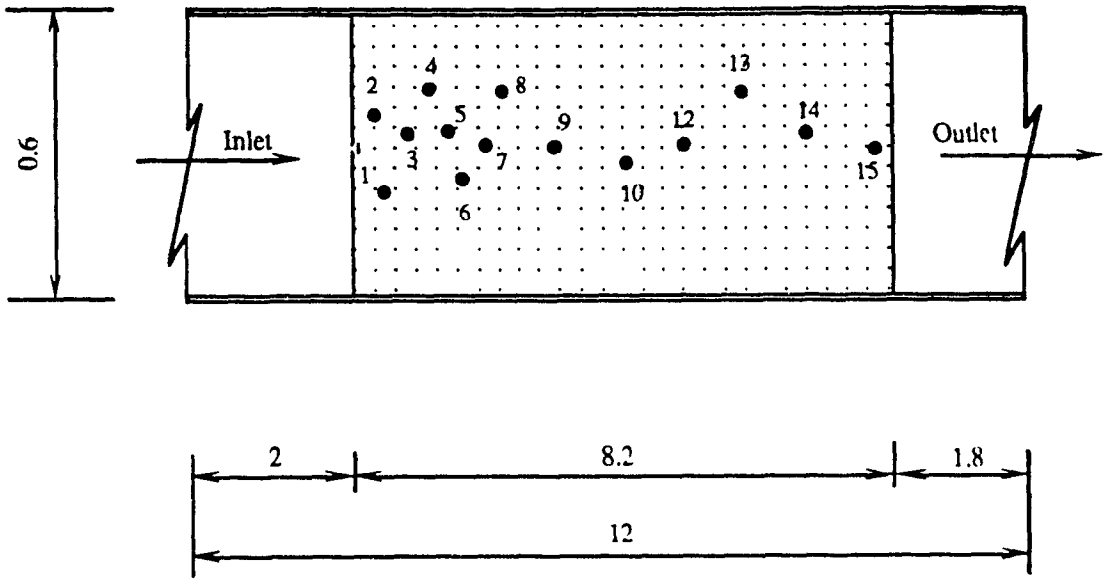

(All dimensions are in m)

Fig. 4.5 Probes distribution over the ice cover in experiment #1

Table 4.1 Distance of each probe from the leading edge

Distance from leading edge					
Probe No.	(cm)	Probe No.	(cm)	Probe No.	(cm)
Probe 1	12.19	Probe 6	112.17	Probe 11	393.19
Probe 2	24.69	Probe 7	137.16	Probe 12	499.87
Probe 3	37.19	Probe 8	162.15	Probe 13	606.55
Probe 4	62.18	Probe 9	187.15	Probe 14	713.23
Probe 5	87.17	Probe 10	286 51	Probe 15	819.91

4.3 Computations Using Existing Formulas

4.3.1 Heat Transfer Coefficient and Its Effect on Ice Melting

Modeling results generated by using the Colburn equation (Eq. (2.14)), the Dittus-Boelter equation (Eq. (2.16)), as well as the Petukhov-Popov equation (Eq. (2.18)) were compared with experimental investigations performed by Hewlett (1976).

The variations of the various heat transfer coefficients along ice cover is shown in Fig. 4.6. Their values are also given in Table 4.2. Fig. 4.6 shows that the three equations have produced constant values of heat transfer

coefficients along the ice cover. The Colburn and the Petukhov-Popov equations gave relatively large values of heat transfer coefficient, with higher values given by the Colburn equation because both account for the roughness of the ice cover bottom surface. However, the Dittus-Boelter equation produced the lowest values of the heat transfer coefficient. This equation does not account for the roughness of the ice surface underside. As can be seen from the Table 4.2 the values produced by using the Colburn equation are about 2 times higher the values given by the Dittus-Boelter equation and about 1.6 times the values yielded using the Petukhov-Popov equation.

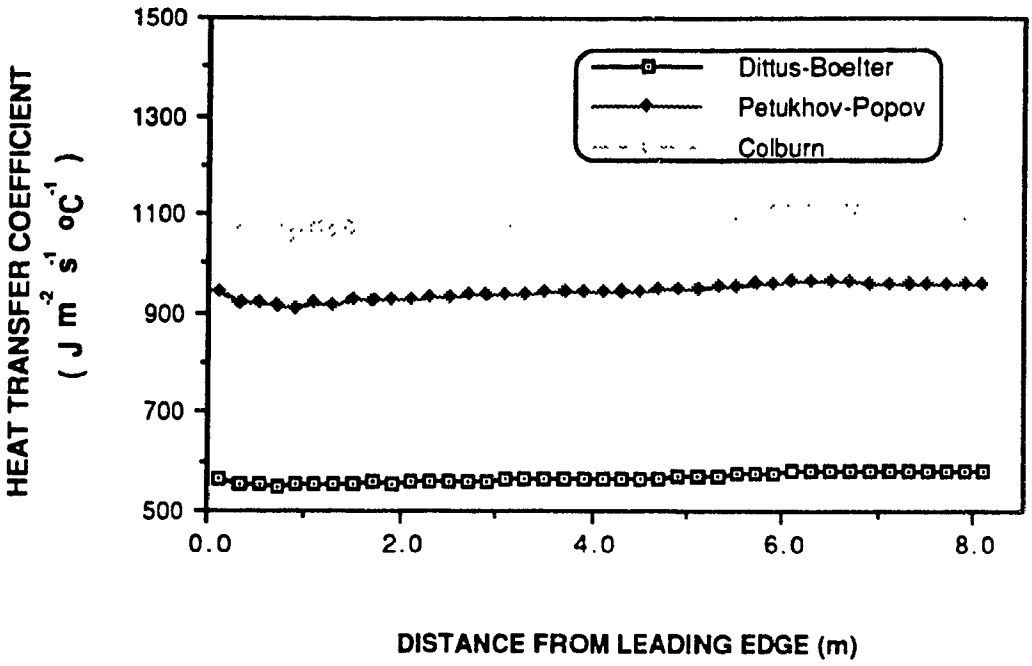

Fig. 4.6 Variations of the heat transfer coefficient using empirical formulas along the ice cover

Table 4.2 Computed values of the heat transfer coefficient along ice cover (J m^{-2} s^{-1} $^{o}C^{-1}$)

Distance from leading edge (m)	Heat transfer coefficient		
	Dittus-Boelter	Colburn	Petukhov-Popov
0.08	561	1093	938
0.1	561	1093	938
0.2	557	1084	929
0.3	553	1072	921
0.5	553	1072	917
0.7	548	1068	917
0.9	553	1059	913
1.1	553	1072	921
1.3	553	1068	917
1.4	553	1072	921
1.6	553	1072	925
2.0	557	1072	934
4.0	565	1072	946
6.0	565	1072	963
8.0	565	1072	963

The effect of the heat transfer coefficient on ice cover melting can be depicted from Figs. 4.7, 4.8, 4.9, 4.10 and 4.11 for probes 1, 2, 3, 11 and 14 respectively. These figures compare computed ice cover thicknesses to experimental observations. Since the ice cover thickness was observed to decrease faster near leading edge, it is important to take closer intervals near this location for comparison, as is the case of probes 1, 2, and 3. Probe 11 was located at about the middle length of the ice cover while probe 14 was near the end of the ice cover. For probe 1 (Fig. 4.7), located at about 0.12 m from the leading edge, the three empirical equations have under-predicted ice melting up to 50 minutes after the starting of computation. After this only the Dittus-Boelter equation continues to yield under-predict results. Fig. 4.7 shows that the Colburn equation has given the closest results while the Dittus-Boelter equation greatly under-predicted ice cover melting. In probe 2, about 0.24 m downstream from leading edge, using the Colburn equation, the model has over-predicted ice melting almost from the beginning. The Petukhov-Popov equation has given the closest results to the experiment while the Dittus-Boelter equation again under-predicted ice melting for this probe much the same for probe 1. Fig. 4.9 shows the same comparison but for probe 3. Both the Colburn and Petukhov-Popov equations have over-predicted ice melting since the beginning, whereas the Dittus-Boelter equation gave the closet results among the three equations. Further downstream as for probes 11 and 14 shown in Figs. 4.10 and 4.11 respectively, the Colburn and the Petukhov-Popov equations have consistently shown over-prediction of ice melting all the time, while the Dittus-Boelter equation gave better agreements with experimental results in this region near the end of the ice cover. In probe 14, the Dittus-Boelter equation has slightly shown an over-prediction of ice cover melting.

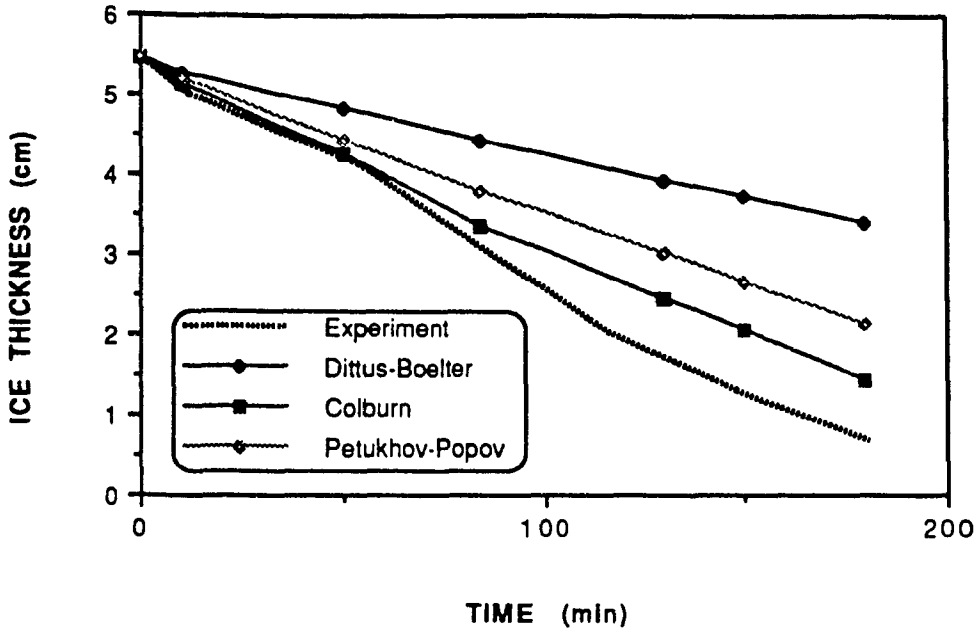

Fig. 4.7 Computed vs measured ice thickness for probe 1

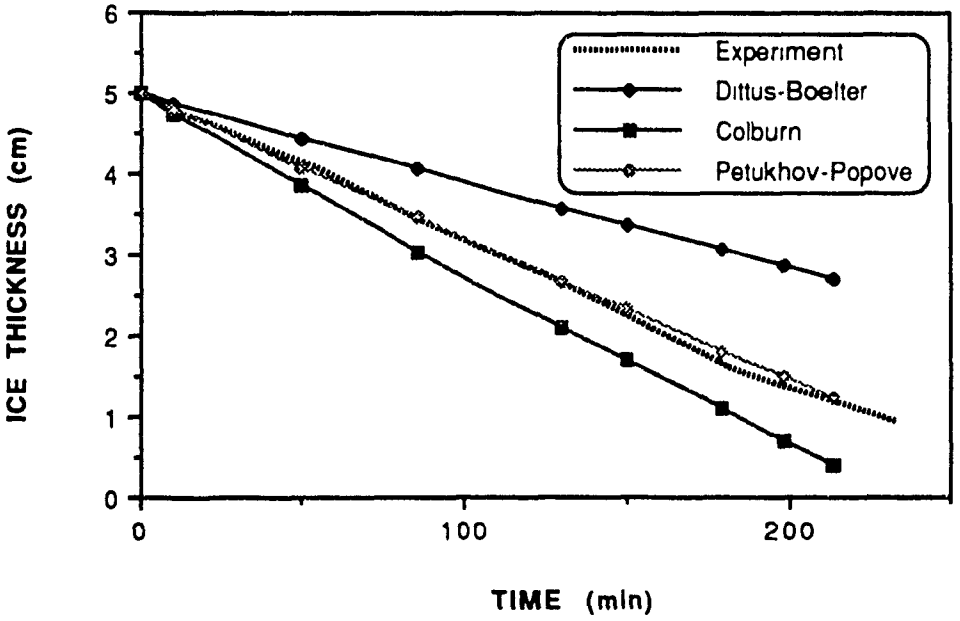

Fig. 4.8 Computed vs measured ice thickness for probe 2

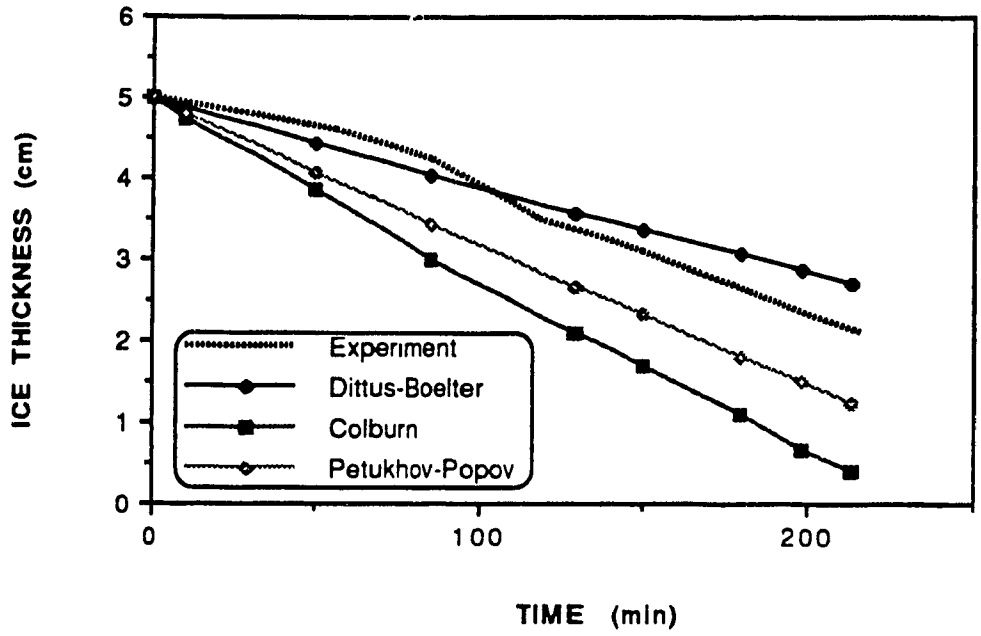

Fig. 4.9 Computed vs measured ice thickness for probe 3

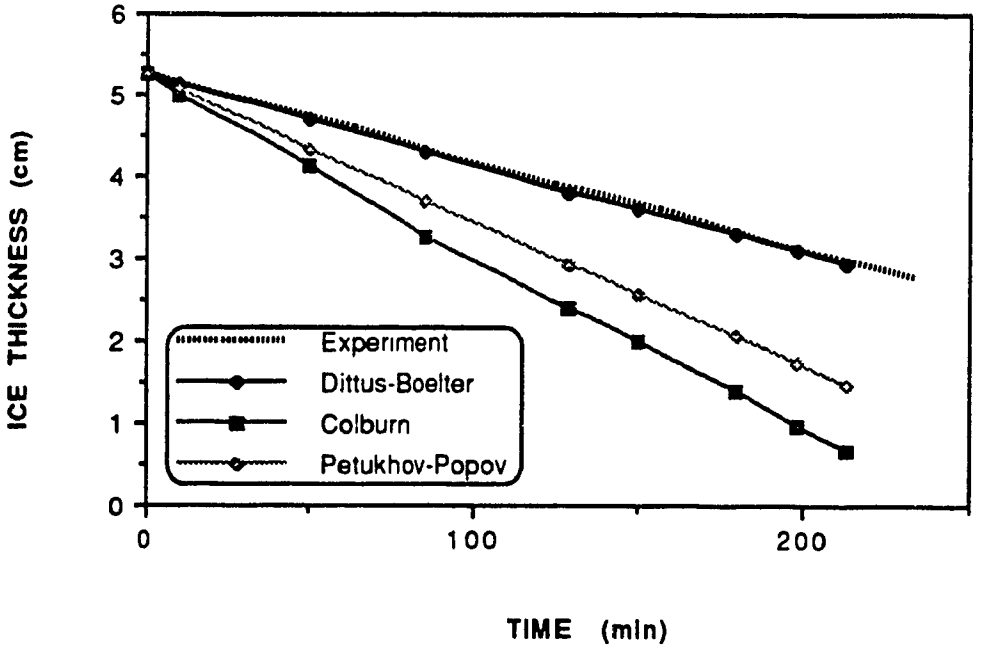

Fig. 4.10 Computed vs measured ice thickness for probe 11

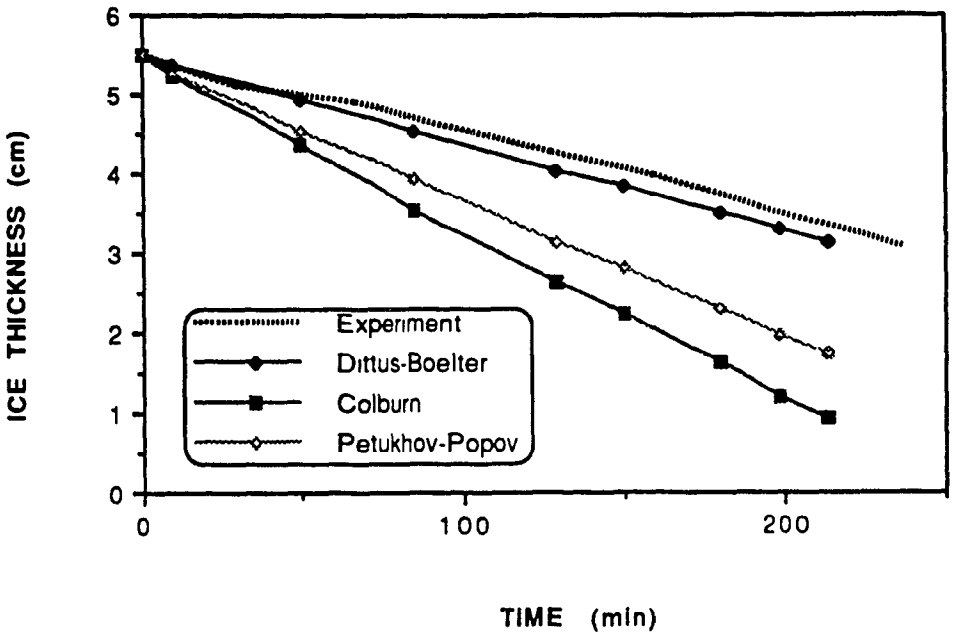

Fig. 4.11 Computed vs measured ice thickness for probe 14

Figs. 4.12 and 4.13 give the ratios of the ice cover thickness using the Colburn and the Petukhov-Popov equations to that of the Dittus-Boelter equation for probes 2 and 14 respectively. The ratios of the Colburn to Dittus-Boelter equation are larger than those of the Petukhov-Popov's due to larger values of heat transfer coefficient produced by the Colburn equation. Since a constant heat transfer coefficient was used, the ratio is increasing with time but at an almost constant rate. The differences of the effects on ice cover thickness due to different heat transfer coefficients used has reached a high of more than 80 percent, as seen from the ratio of the Colburn to Dittus-Boelter equation for probe 14.

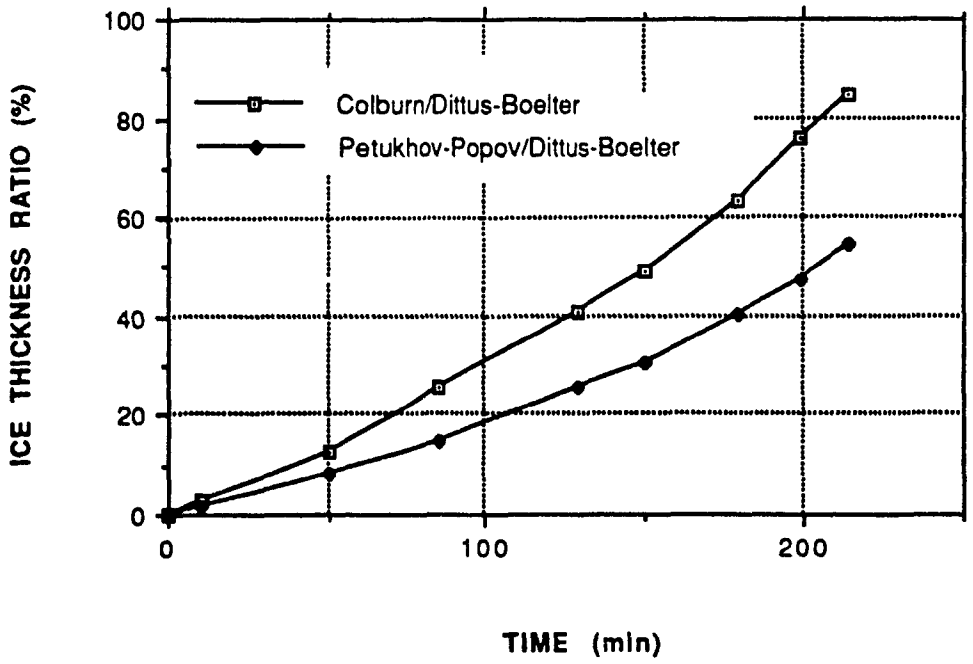

Fig. 4.12 Ratios of the ice thickness for probe 2

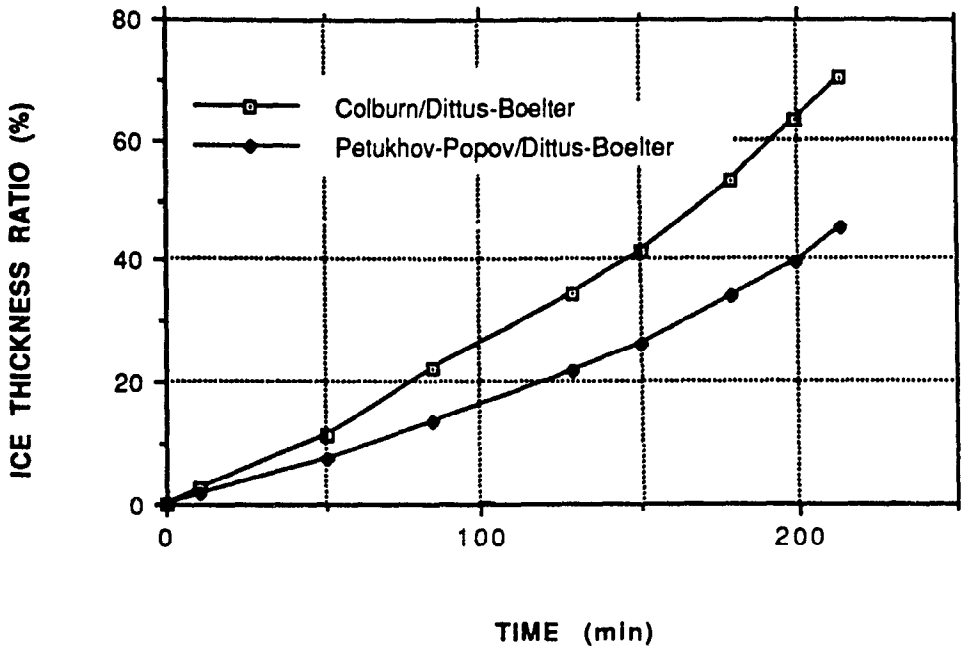

Fig. 4.13 Ratios of the ice thickness for probe 14

Figs. 4.14 and 4.15 present the profiles of the ice cover thickness at time 100 and 200 minutes, respectively. As shown in these figures the Dittus-Boelter equation gave the best predictions among the three equations. The Colburn and the Petukhov-Popov equations over-predicted the ice melting seriously from the very beginning. It is also noted three profiles of the ice cover thickness from the empirical equations are parallel, resulted again from the constant heat transfer coefficient. The variations of the ice thickness in time averaged over the length of the ice cover are given in Fig. 4.16. The Dittus-Boelter equation has yielded the best results most of the time.

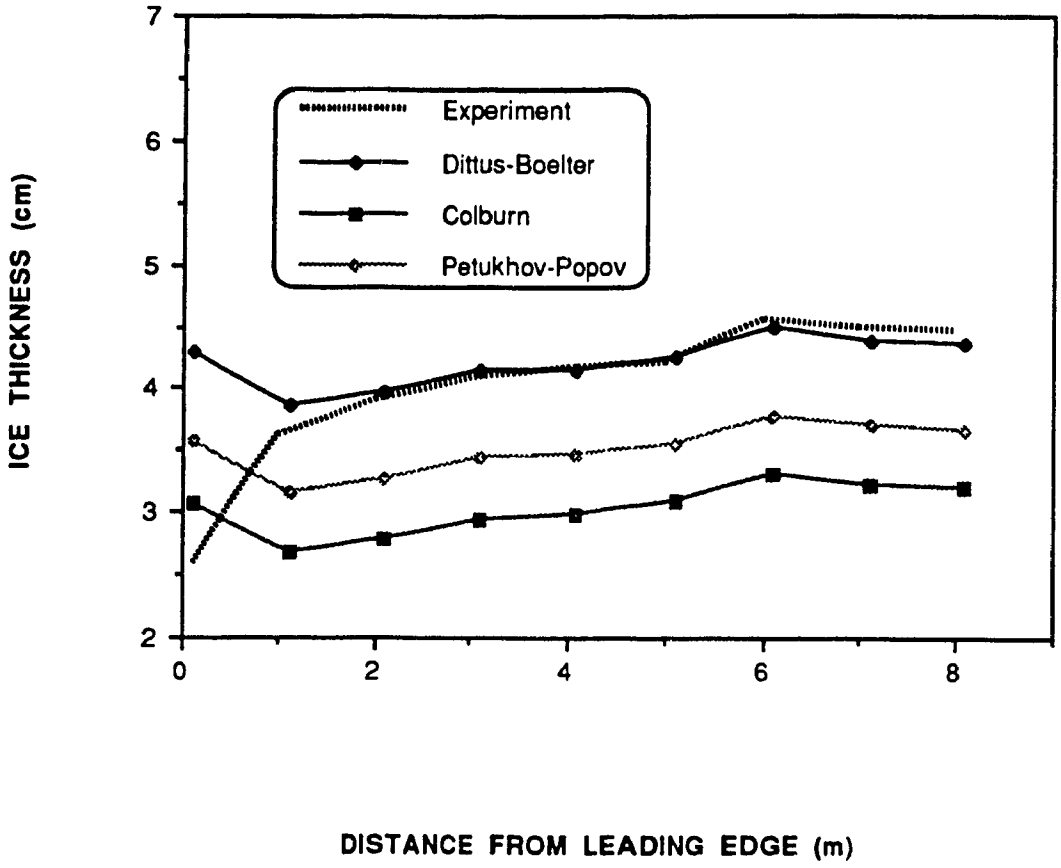

Fig. 4.14 Computed vs measured ice thickness profiles at time 100 minutes

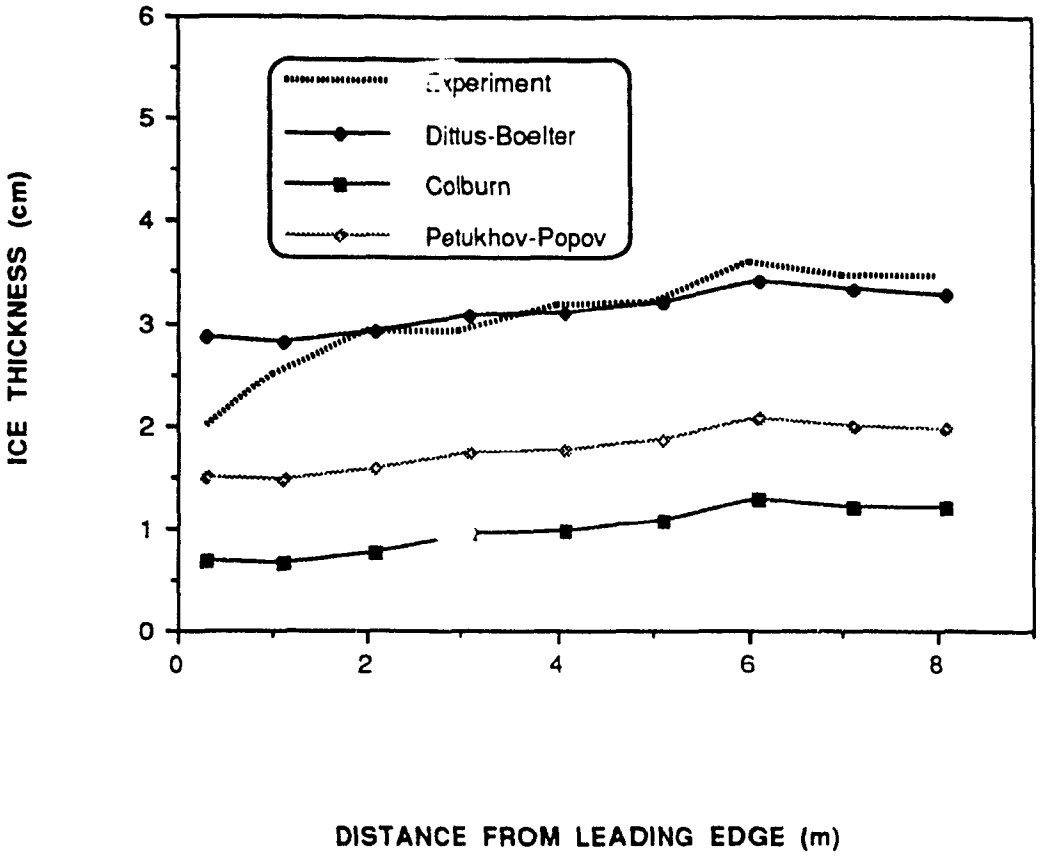

Fig. 4.15 Computed vs measured ice thickness profiles at time 200 minutes

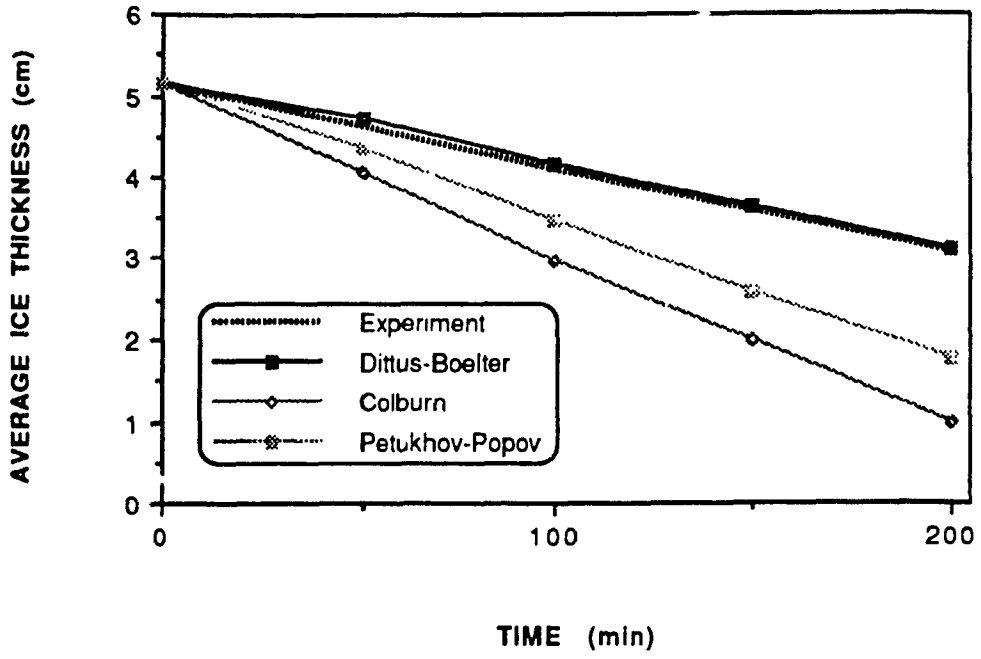

Fig. 4.16 Computed vs measured ice thickness averaged over distance

4.3.2 Melting Rate of the Ice Cover

The effect of the heat transfer coefficient can also be gauged by considering the ice melting rate. Fig. 4.17 shows the variations of ice melting rate at different probes. The values of the melting rate are presented in Table 4.3. Fig. 4.17 shows that the computed ice melting rates are constant along the ice cover. The Colburn equation produced the largest values of the melting rate, which were about twice the values of the Dittus-Boelter equation. The Petukhov-Popov equation generated values of 1.6 times the Dittus-Boelter equation. The Dittus-Boelter equation resulted in larger than observed ice melting rate beyond probe 9 in the downstream direction, about 1.9 m from

the leading edge. The Colburn equation produced over-predicted values of the melting rate at probe 2 and beyond.

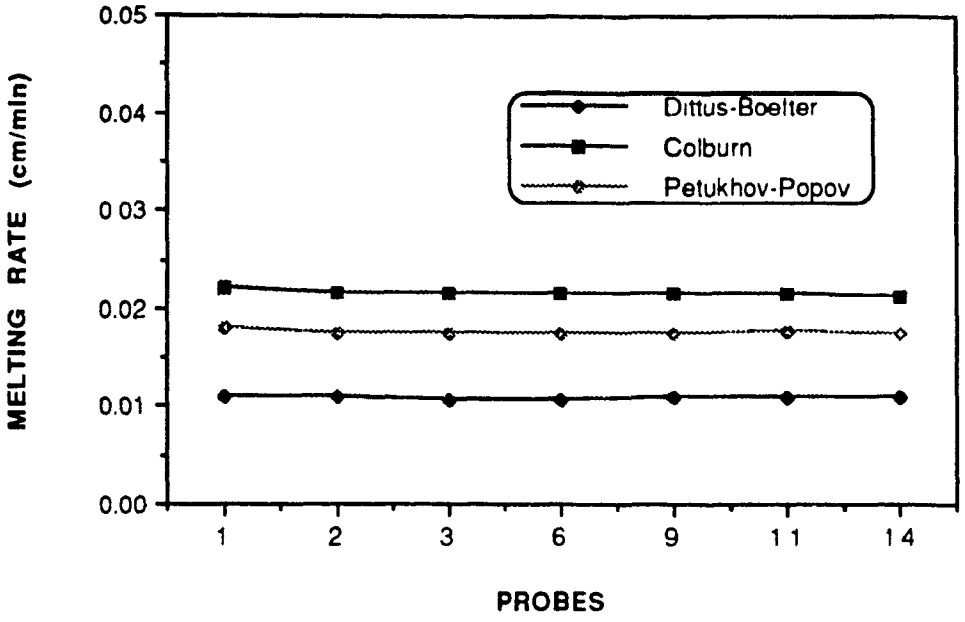

Fig. 4.17 Variations of melting rates from empirical formulas

Table 4.3 Mean values of the computed and measured ice melting rate at different probes (cm/min)

Probe No.	Experimental Results	Computational Results		
		Dittus-Boelter	Colburn	Petukhov-Popov
Probe 1	0.0270	0.0110	0.0220	0.0179
Probe 2	0.0210	0.0108	0.0216	0.0176
Probe 3	0.0160	0.0107	0.0215	0.0175
Probe 6	0.0120	0.0107	0.0215	0.0175
Probe 9	0.0100	0.0108	0.0215	0.0176
Probe 11	0.0100	0.0108	0.0215	0.0177
Probe 14	0.0100	0.0109	0.0214	0.0176

4.3.3 Water Temperature and Depth

The variations of computed water temperature along the channel beneath the ice cover are shown in Figs. 4.18 and 4.19 for 100 and 200 minutes, respectively. The water temperature resulted from using the Colburn equation was much lower than the other equations. However, the highest values of the temperature profile along the channel were obtained by using the Dittus-Boelter equation. At the leading edge, the water temperature resulted from the use of the Dittus-Boelter and the Petukhov-Popov equations were about 1 ^{o}C. The Colburn equation generated the water temperature below 1 ^{o}C due to higher heat losses. At time 200 minutes, the

water temperature gradient obtained from the Dittus-Boelter and Petukhov-Popov equations were lower than those at time of 100 minutes, indicating larger heat transfer from water to the ice due to thinning of the ice. By using the Colburn equation the water temperature at 200 minutes was higher than before because most of the ice cover has melted.

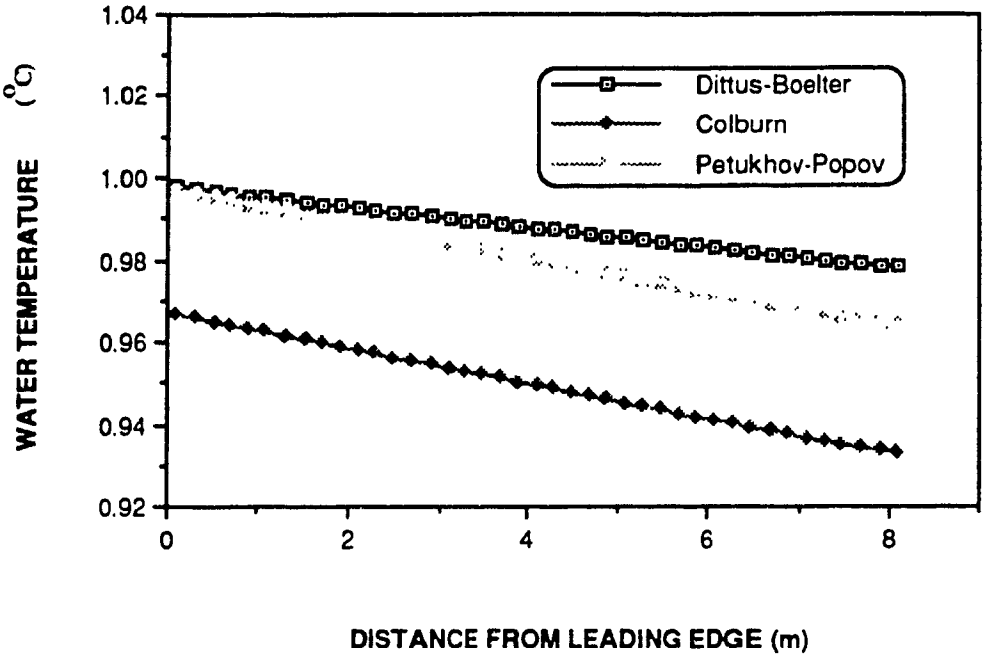

Fig. 4.18 Computed water temperature variations at time 100 min

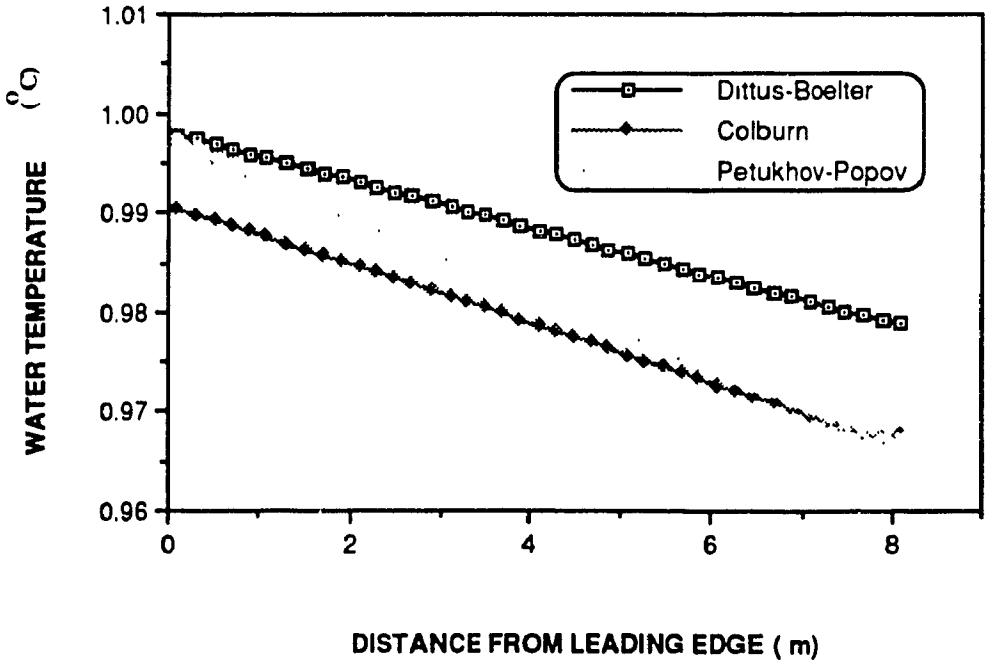

Fig. 4.19 Computed water temperature variations at time 200 min

Figs. 4.20 and 4.21 show the variations of water depth under ice cover at time 100 and 200 minutes respectively. In these figures the water depths obtained using the Colburn equation are the highest due to higher ice melting rate than that from the other two equations. At time 200 minutes the water depths generated using the three equations were higher than those by about 6% at time 100 minutes due to the ongoing melting of the ice cover.

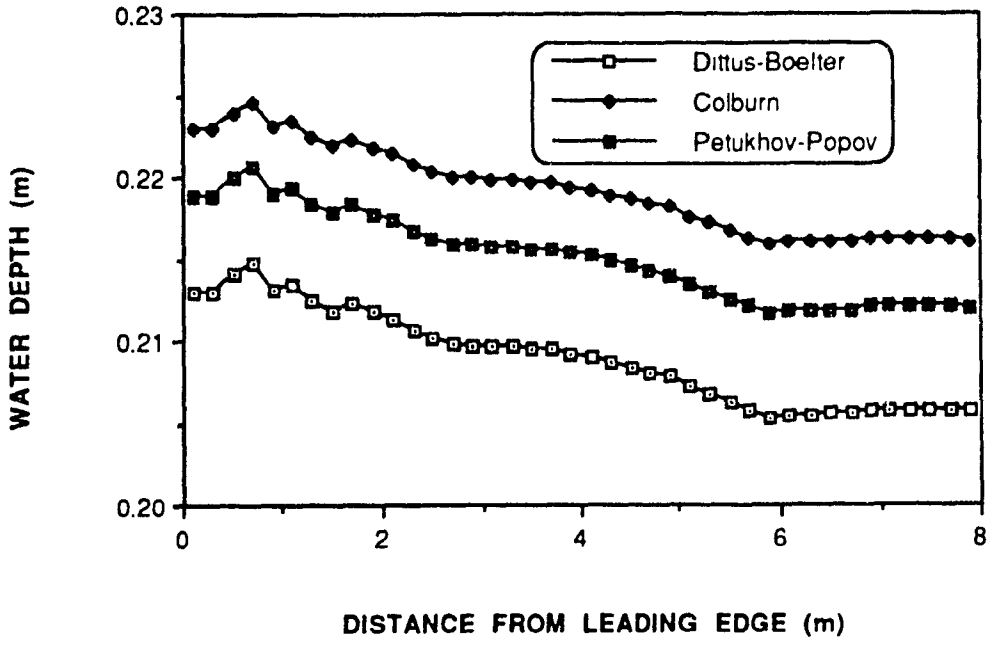

Fig. 4.20 Computed water depth variations at time 100 min

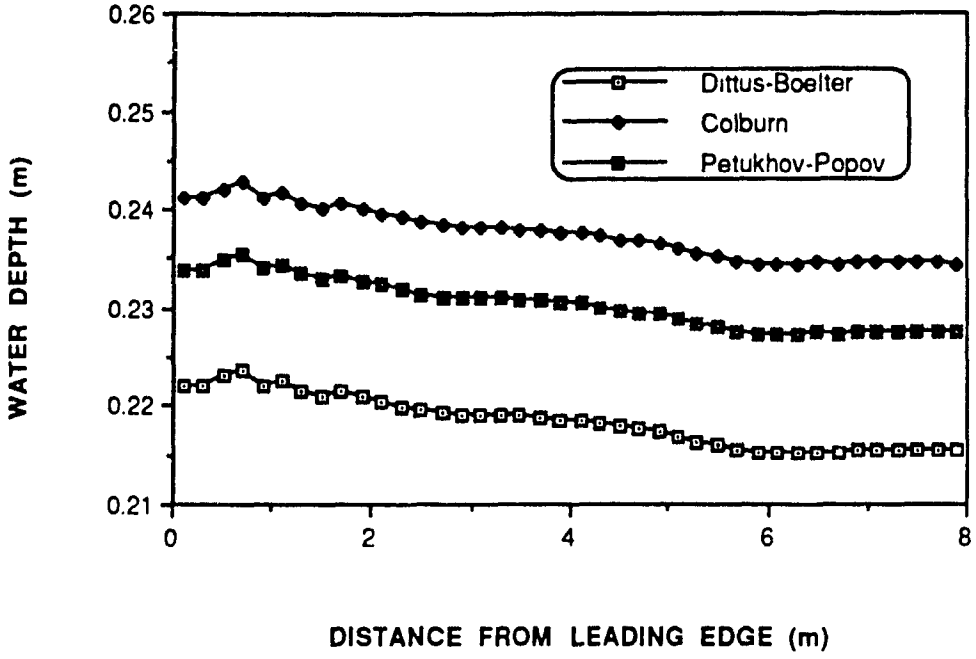

Fig. 4.21 Computed water depth variations at time 200 min

4.4 Results from New Formula

4.4.1 Heat Flux

The variations of the heat transfer coefficient produced using the new formula (Eq. (2.36)) were compared to those of the experiment and the three empirical equations as well. These variations are shown in Fig. 4.22. Table 4.4 lists the values of the coefficient along the ice cover. As shown in Fig. 4.22, in contrast to the empirical formulas, the variations of the heat transfer coefficient along the ice cover given by the new formula fit better with the experimental results. They have large values near the leading edge and smaller ones toward the end of the ice cover. Actually, the variations of the heat transfer coefficient can be divided into two distinct zones along the ice cover. In the entry zone, within the length of about 0.5 m from the leading edge, the values of the heat transfer coefficient show rapid decrease with distance. In the immediate neighborhood of this zone, which can be called transition zone, the heat transfer coefficient varied rather gradually with distance. The ratios of the heat transfer coefficients from experiment to all equations are shown in Figs. 4.23 and Table 4.5. Fig. 4.23 shows that the Dittus-Boelter equation got quite large ratio near the leading edge but better results afterward. Both the Colburn and Petukhov-Popov equations had smaller values than the Dittus-Boelter equation near the leading edge but much larger downstream. The new formula generated smaller ratio values than the Dittus-Boelter and Petukhov-Popov equations near the leading edge and much closer values of the heat transfer coefficient to experiment for the rest of the ice cover.

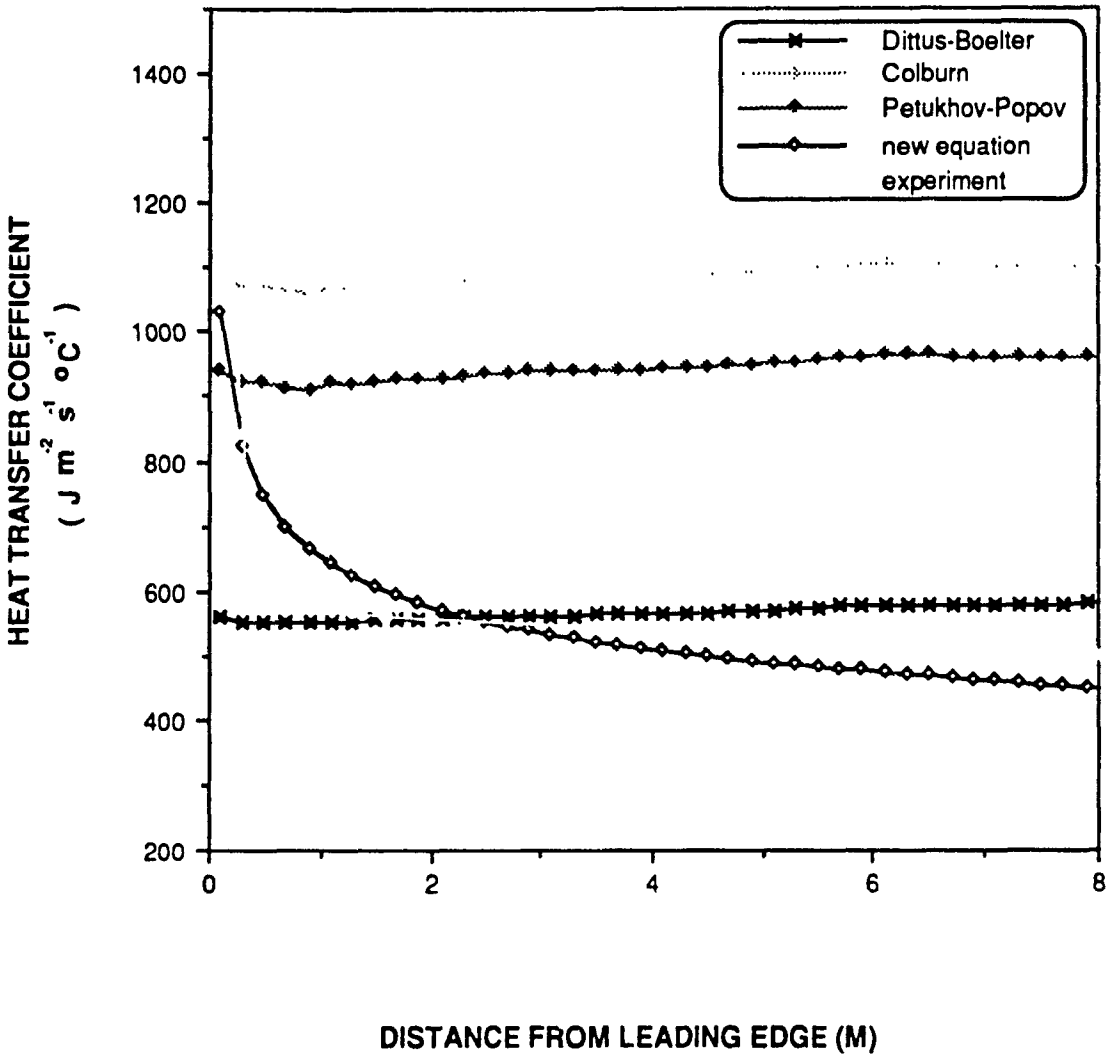

Fig. 4.22 Computed vs measured heat transfer coefficient

Table 4.4 Mean values of the heat transfer coefficient from new formula and experiment along ice cover (J m^{-2} s^{-1} $^{o}C^{-1}$)

Distance from the leading edge (m)	Heat transfer coefficient	
	New formula	Experiment
0.08	1097	1340
0.1	1030	1294
0.2	925	1055
0.3	825	846
0.5	749	641
0.7	699	607
0.9	666	590
1.1	645	578
1.3	624	569
1.4	615	565
1.6	599	561
2.0	574	557
4.0	511	540
6.0	477	519
8.0	448	498

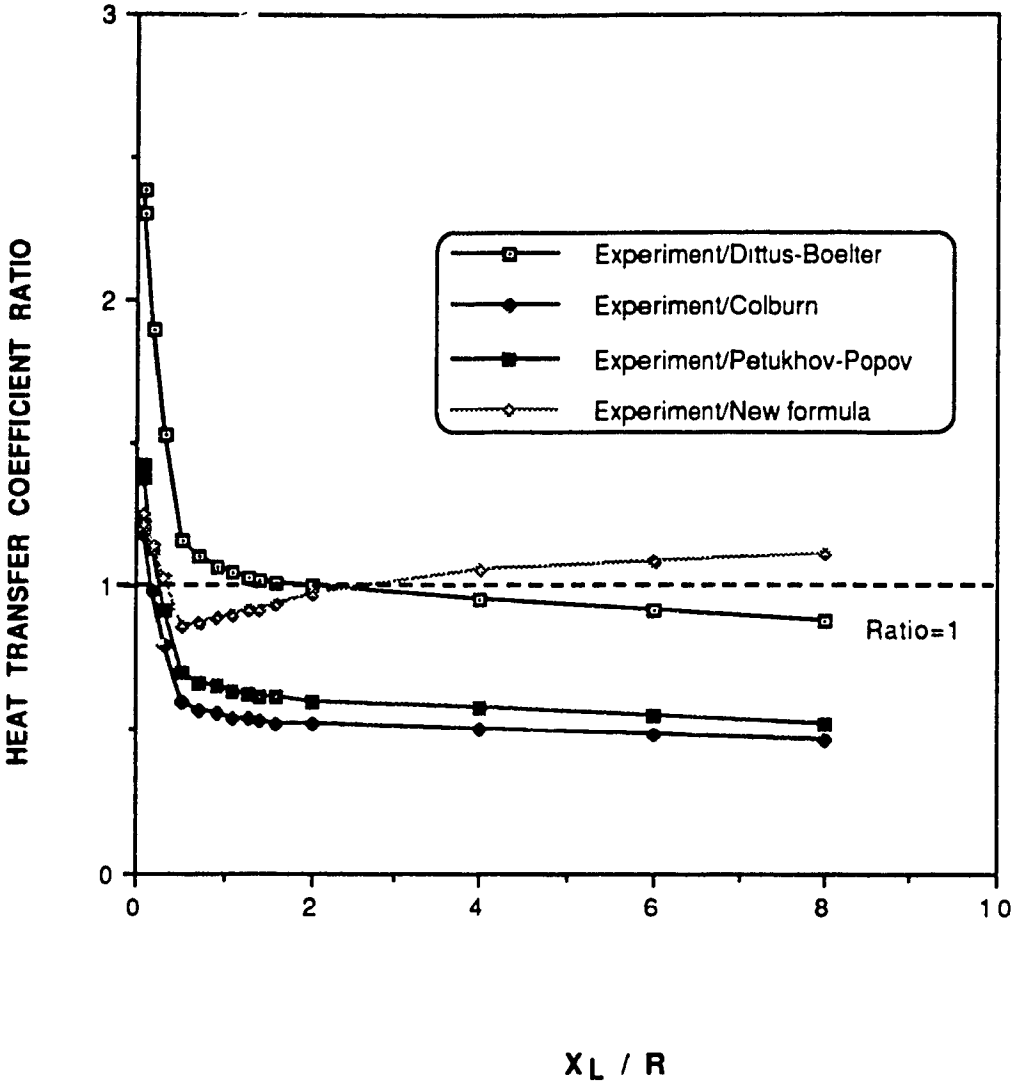

Fig. 4.23 Ratios of measured to computed heat transfer coefficients

Table 4.5 Ratio of experimental heat transfer coefficient to computed values

x_1 / R	1	5	10	15	20	25	30	35
Ratio								
New formula	1.26	0.86	0.89	0.93	0.97	1.03	1.04	1.00
Dittus-Boelter	2.31	1.16	1.05	1.01	1.00	1.02	1.00	0.93
Colburn	1.18	0.60	0.55	0.52	0.52	0.53	0.52	0.48
Petukhov-Popov	1.38	0.70	0.63	0.61	0.60	0.61	0.60	0.55

The percentage differences between computed and measured heat transfer coefficients are given in Table 4.6. The standard deviations (σ_{n-1}) of these differences are presented in Table 4.7. Clearly, the new formula had the closest values of the heat transfer coefficient to the experiment and gave the smallest values of deviation among all the equations. Both the Colburn and Petukhov-Popov equations had large differences and deviations as well. The Dittus-Boelter equation shows larger differences than both the Colburn and Petukhov-Popov within first 0.3 m from the leading edge but closer values of the heat transfer coefficient to the experiment afterward.

Table 4.6 Differences between computed and measured heat transfer coefficient (%)

Distance from the leading edge (m)	Differences (%)			
	Dittus-Boelter	Colburn	Petukhov-Popov	New formula
0.08	- 58.8	- 18.4	- 30.0	- 18.1
0.1	- 56.6	- 15.5	- 27.5	- 20.4
0.2	- 47.2	2.8	- 11.9	- 12.3
0.3	- 34.5	26.7	9	- 2.5
0.5	- 13.5	67.3	43.7	17
0.7	- 9.1	75.9	50.8	15.1
0.9	- 6.2	79.4	54.3	12.8
1.1	- 4.0	85.5	59.4	11.6
1.3	- 2.9	87.5	61.2	9.6
1.4	- 2.1	89.6	63.5	8.9
1.6	- 0.8	91.0	64.7	6.7
2.0	0	92.5	67.7	3.0
4.0	4.7	98.4	75.0	- 5.4
6.0	8.9	106.5	85.3	- 8.1
8.0	13.4	115	92.9	- 10.1

Table 4.7 Standard deviations of difference between computed and measured heat transfer coefficient (%)

Standard deviation (σ_{n-1})			
Dittus-Boelter	Colburn	Petukhov-Popov	New formula
23.6	44.2	39.7	12.3

Fig. 4.24 and Table 4.8 show the ratio of the heat transfer coefficient of the new formula to that of the three empirical formulas, in which X_L is the length from the leading edge and R is hydraulic radius. As shown in Fig. 4.24 that, near the leading edge, the heat transfer coefficient from the Dittus-Boelter equation is about 1.83 times the values from the new formula but with closer values obtained downstream. Both the Colburn and Petukhov-Popov equations have closer values than the Dittus-Boelter equation in the leading edge, however, about 1.5 times the new formula after 1 m downstream from the leading edge.

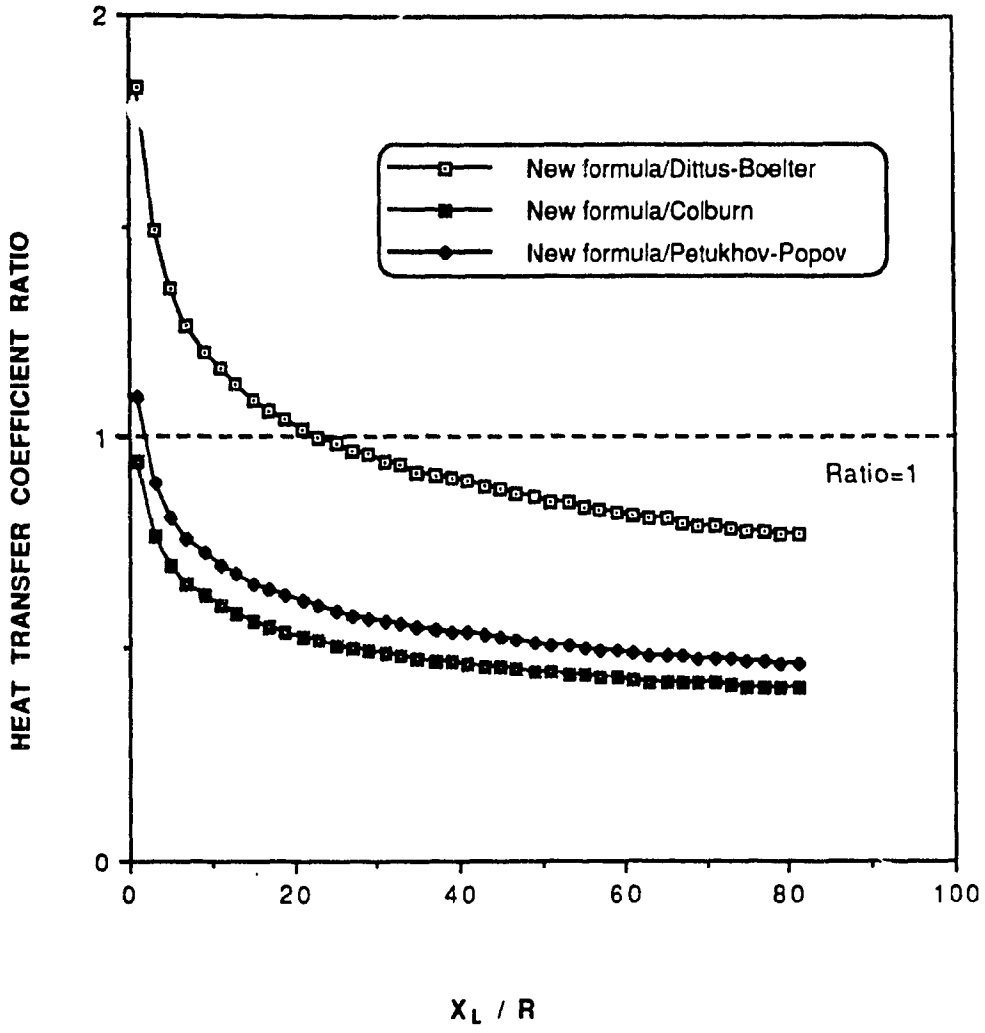

Fig. 4.24 Ratios of heat transfer coefficient from the new formula to empirical formulas

Table 4.8 Ratio of the heat transfer coefficient from new formula to empirical formulas

x_1 / R	1	5	10	15	20	25	30	35
	Ratio							
Dittus-Boelter	1.83	1.36	1.17	1.10	1.03	0.99	0.96	0.93
Colburn	0.94	0.70	0.61	0.57	0.54	0.51	0.49	0.49
Petukhov-Popov	1.10	0.81	0.71	0.66	0.62	0.59	0.57	0.57

4.4.2 Melting Rate of the Ice Cover

Table 4.9 lists the mean values of ice melting rate from the experiment and the new formula along the ice cover. A comparison of computed melting rates from all equations to those of experiment at different probes along the ice cover is shown in Fig. 4.25. The melting rate computed using the new formula reflects the thermal entrance influence and gives a better agreement with the experiment, being large at the leading edge and small near the end of the ice cover. The differences in melting rate between experiment and computations are presented in Table 4.10 and Table 4.11, showing the standard deviation (σ_{n-1}) of differences of the melting rates.

Table 4.9 Mean values of ice melting rates over time using the new formula (cm/min)

Probe No.	Experiment	New formula
Probe 1	0.0270	0.0201
Probe 2	0.0210	0.0162
Probe 3	0.0160	0.0146
Probe 6	0.0120	0.0125
Probe 9	0.0100	0.0113
Probe 11	0.0100	0.0100
Probe 14	0.0100	0.0091

Table 4.10 Differences of melting rate between computations and experiment

Difference (%)				
Probe No.	Dittus-Boelter	Colburn	Petukhov-Popov	New formula
Probe 1	- 59.3	- 18.5	- 33.7	- 25.6
Probe 2	- 48.6	2.9	- 16.2	- 22.9
Probe 3	- 33.1	34.4	9.4	- 8.8
Probe 6	- 10.8	79.2	45.8	4.2
Probe 9	8	115	76	13
Probe 11	8	115	76	0
Probe 14	9	114	76	-9

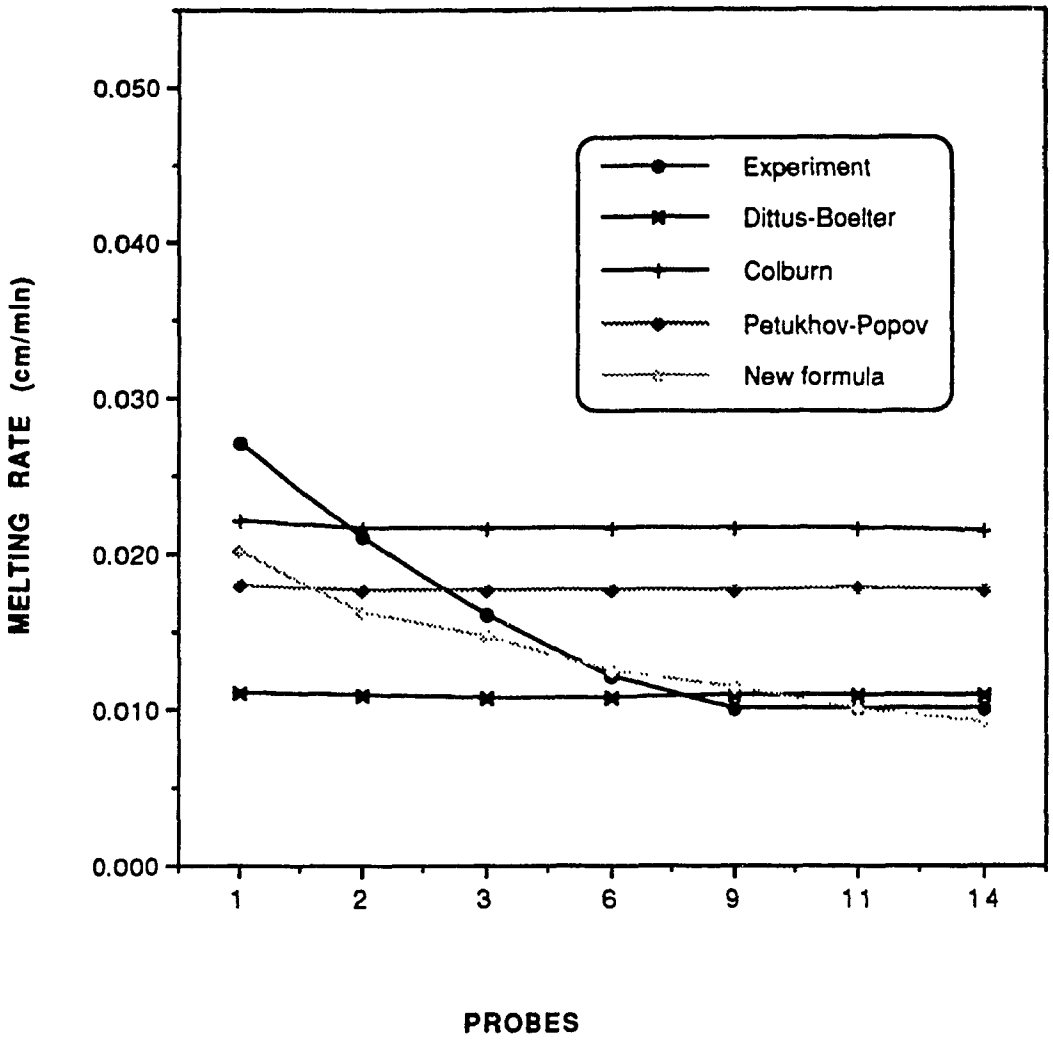

Fig. 4.25 Computed vs measured melting at different probes

Table 4.11 Standard deviations of the difference in the melting rate (%)

Standard deviation (σ_{n-1})			
Dittus-Boelter	Colburn	Petukhov-Popov	New formula
28.9	56.8	48.9	14.0

The standard deviation of the error using the new formula is shown to be the smallest among the four equations. The Dittus-Boelter equation has also given noticeably smaller value than those of the other two empirical equations.

4.5 Field Comparison and Discussions

The numerical model was also applied to the field case using three empirical equations, Dittus-Boelter equation, Colburn equation and Petukhov-Popov equation. Computational results were compared to the field data of Feb. 17, 1980, which was carried out by the U.S. Army Cold Regions Research and Engineering Laboratory, Hanover, N.H., U.S.A. The field study

was performed on the melting of river ice by a side thermal discharge on the Mississippi River near Bettendorf, Iowa.

The field investigation was conducted from February 13 to 18, 1980 on the Mississippi River ice suppression due to thermal effluent. All together there were 16 locations at which field measurements were taken along the river in the study site. Field measurements included water velocity, temperature, and water depth. The open water reach was determined from aerial overflights photos. Tabel 4.12 presents each site measurements location and names. The location of the origin is defined at somewhere upstream of the river. The measurements location name and origin are shown in Fig. 4.26. For the water velocity and depth, only some of field measured data are available. Water velocities were measured at the edge of the ice cover at different water depth. In the comparison of the field data to computational results, the depth averaged water velocity from field data was used. Water depth measurements were taken within certain distance from shore in the field.

The Mississippi River, at the field study, is approximately 1 km in width and 12km long in longitudinal direction. The water depth varied between a minimum of 2 m and a maximum of 10 m with a gradual increase in the downstream direction. The river flow discharge during the study was about 850 m^3/s with the mean flow velocity of about 0.25 m/s. The geometry of the river in study site and location of the thermal discharge from the power plant, which is approximately 3 km longitudinal direction from the entrance, are illustrated by Fig. 4.26. The elevation contour line of the river bed is shown in Fig. 4.27, in which z stands for the bed elevation above an

arbitrary datum. Both discharges in the entrance and from power plant were exactly reproduced in the model. The river bed elevation was also taken into account in the modelling.

Table 4.12 Site measurement name and location

Location name	Longitudinal direction from origin (m)
BB-B	-216
BRM-0	0
DBRM-1	320
BH-2	970
PRN-3	1530
MLD-4	2173
TAT-5	2980
TLD-6	3510
PLD-7	4260
SLD-8	4590
UCP-9	5130
CT-10	5346
IBRG-11	6450
INDC-12	7342
ULP-13	8290
BDB-14	8640

Three hour meteorological records, including air temperature, cloud cover tenths, wind velocity and vapour pressure, were taken from the Molin, Illinois airport weather office located 6 miles from the study site. Table 4.13 presents meteorological conditions for the 17th of February, 1980. On the 17th the colder air temperature affected lengthening open water reach. In the computations, the daily average meteorological conditions were considered.

Table 4.13 Meteorological conditions of Feb. 17,1980

Air temperature (°C)	- 18.75
Cloud cover (tenths)	0.0
Latitude (degrees)	41.5
Wind velocity (m/s)	3.99
Vapour pressure (mb)	1.05

The thermal effluent discharge, originated from the riverside power plant, was almost constant during the study period with the average temperature of 8.9°C. Inflow water temperature was slightly above 0°C at the entrance to the study reach. The value of 0.05°C of inflow water temperature was used and average water temperature of 8.9°C from power plant was considered in the model.

Ice cover edge locations were determined from oblique aerial photographs. The river was originally covered with ice extended from

upstream to downstream over a whole width of the river. An initial average ice thickness of 0.25m was taken as an initial simulation condition in the modeling.

Figures 4.28, 4.29 and 4.30 show ice thickness distribution from modeling. Contour line of 0.25m ice thickness from using three empirical equations is shown in Fig. 4.31. In the figures solid black line stands for the initial ice thickness of 0.25m and z presents value of ice thickness. As can be seen the original ice thickness of 0.25m contour line, near thermal effluent, moved away from the shore. This results indicate that ice thickness within this closed contour line area is thinner than 0.25m after suppression of the river ice occured. Results from using the Colburn equation show the contour line of 0.25m extends up to about 6.9km downstream from thermal effluent source. While results from the Dittus-Boelter equation has a stretch of about 3.7km and from the Petukhov-Popov equation about 5.8km. This implies that the Colburn equation produced the largest heat transfer coefficient, resulting in more ice melting than those of other two.

Water temperature distribution generated from three equations are shown in Figs. 4.32, 4.33 and 4.34. Fig. 4.35 presents 0.14°C contour line near thermal discharge. Results show the Colburn equation has 3.1km in length of 0.14°C contour line. The extended contour line of 0.14°C from the Dittus-Boelter equation and the Petukhov-Popov equation are 5.8km and 3.5km respectively. The closed contour line area from the Colburn equation is the smallest because more heat transfered from water to ice cover, resulting in lowering water temperature. Contrarily, the contour line area is the largest in

the case of using the Dittus-Boelter equation due to small heat flux from water to ice cover.

Water depth comparison between computations and field measurements at different location is presented in Figs. 4.36 to 4.38. These figures show that computations have a good agreement with field measurements. Three modelling results by adapting three equations do not have big difference in water depth calculation. The average values of water depth in longitudinal direction are given by Table 4.14.

Table 4.14 Mean water depth in Mississippi River (m)

Mean water depth (m)	
Field measurement	2.92
Dittus-Boelter equation	2.89
Colburn equation	2.93
Petukhov-Popov equation	2.92

Figure 4.39 to Fig 4.41 show water flow velocity from modelling compared to field measurements at different location. Computational results have the good agreement with field data. Three equations produced results close to each other in velocity.

Table 4.15 Mean water flow velocity in Mississippi River (s/m)

Mean water velocity (s/m)	
Field measurement	0.248
Dittus-Boelter equation	0.236
Colburn equation	0.222
Petukhov-Popov equation	0.220

The comparison of ice free reach from modeling to the field data also shows that that the Colburn equation generated the closest results to the field study. The values of ice free reach from modeling and field study are listed in Table 4.16. The Petukhov-Popov Equation also produced closer results to field measurements than that of the Dittus-Boelter Equation.

Table. 4.16 Values of ice free reach for Mississippi River (km)

Length of ice free reach (km)	
Field measurement	4.3
Dittus-Boelter Equation	2.1
Colburn Equation	2.7
Petukhov-Popov Equation	2.4

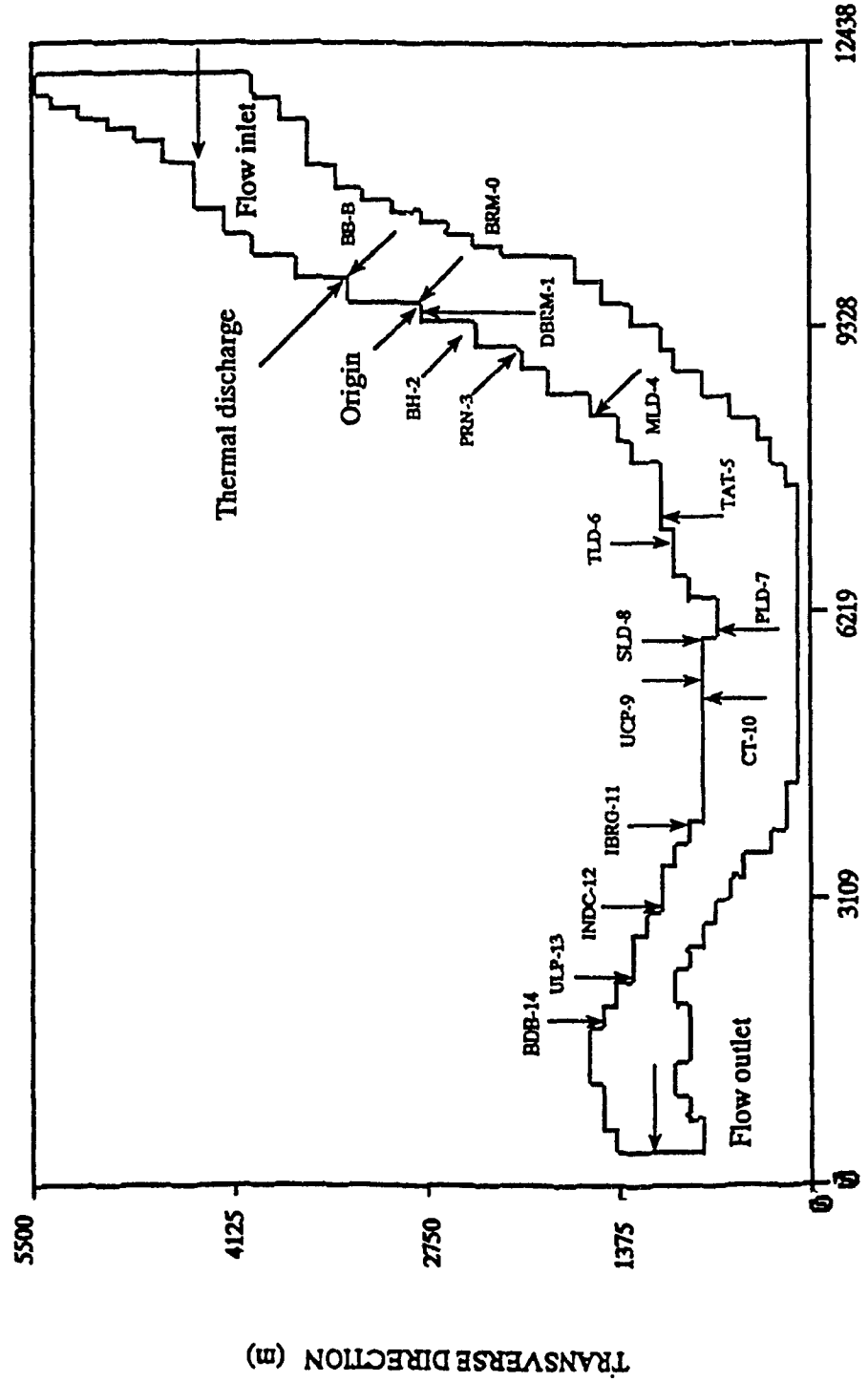

Fig. 4.26 Mississippi River geometry of study site

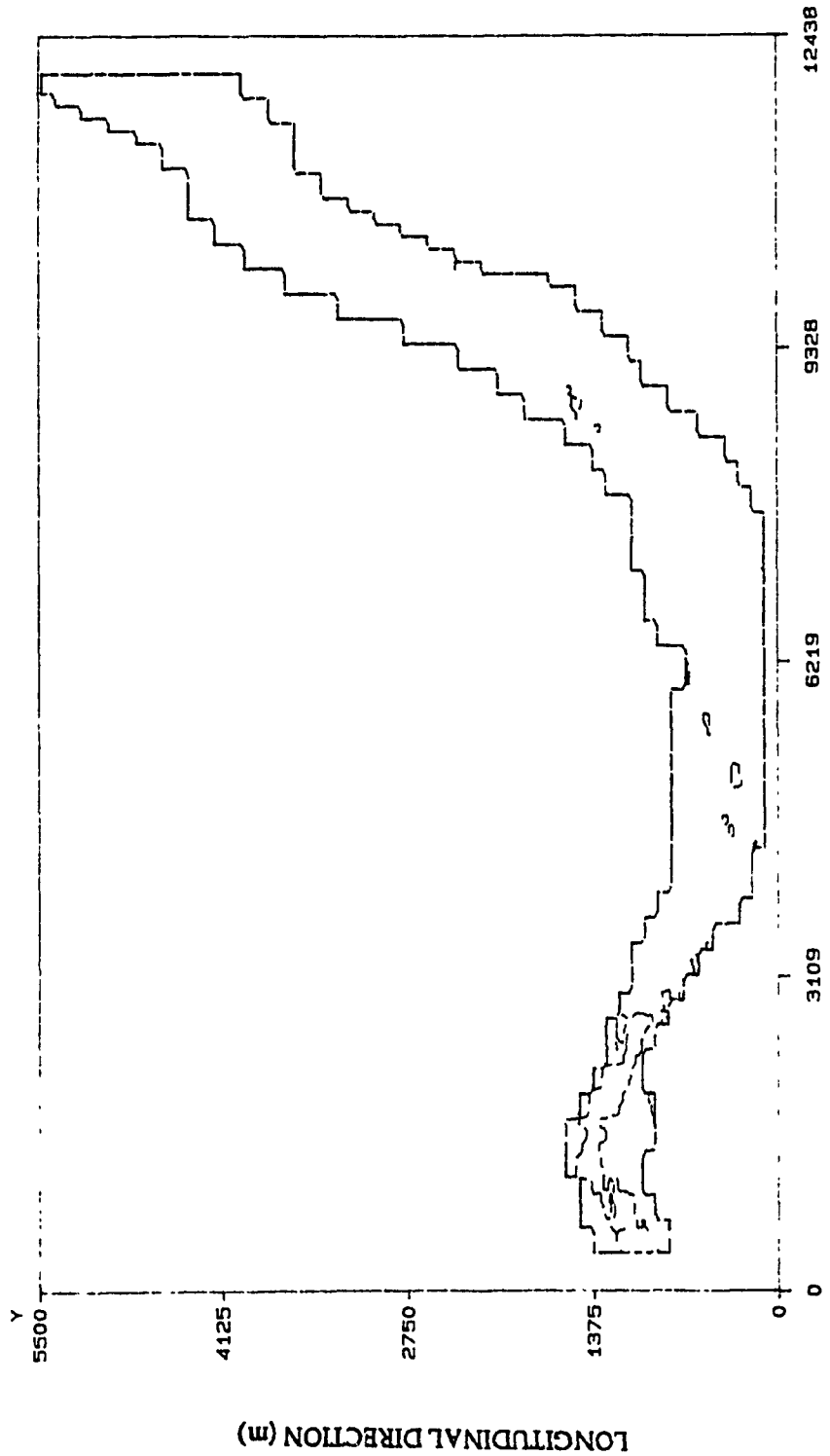

Fig. 4.27 Mississippi River bed elevation

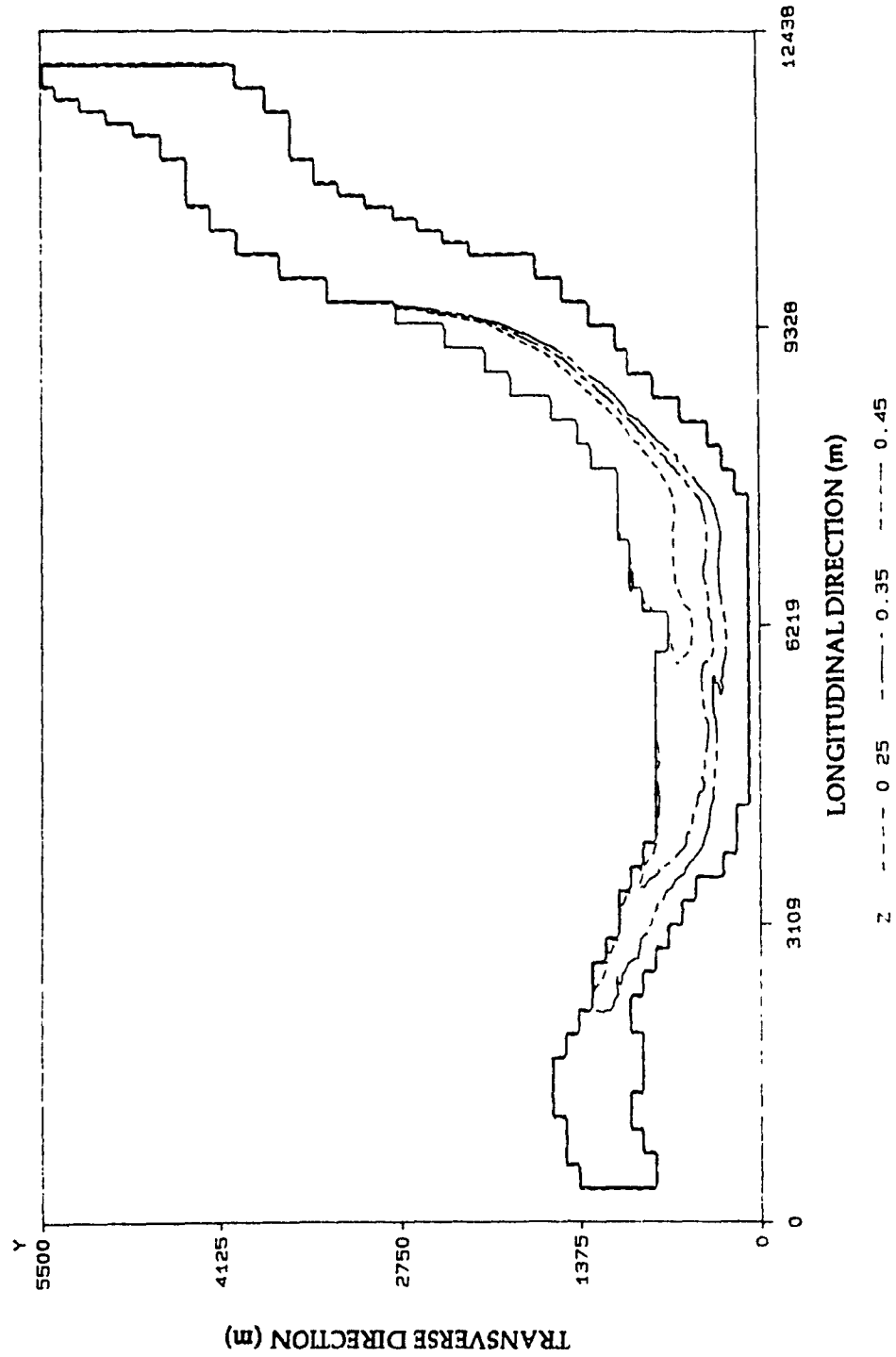

Fig. 4.28 Ice thickness distribution from Dittus-Boelter equation

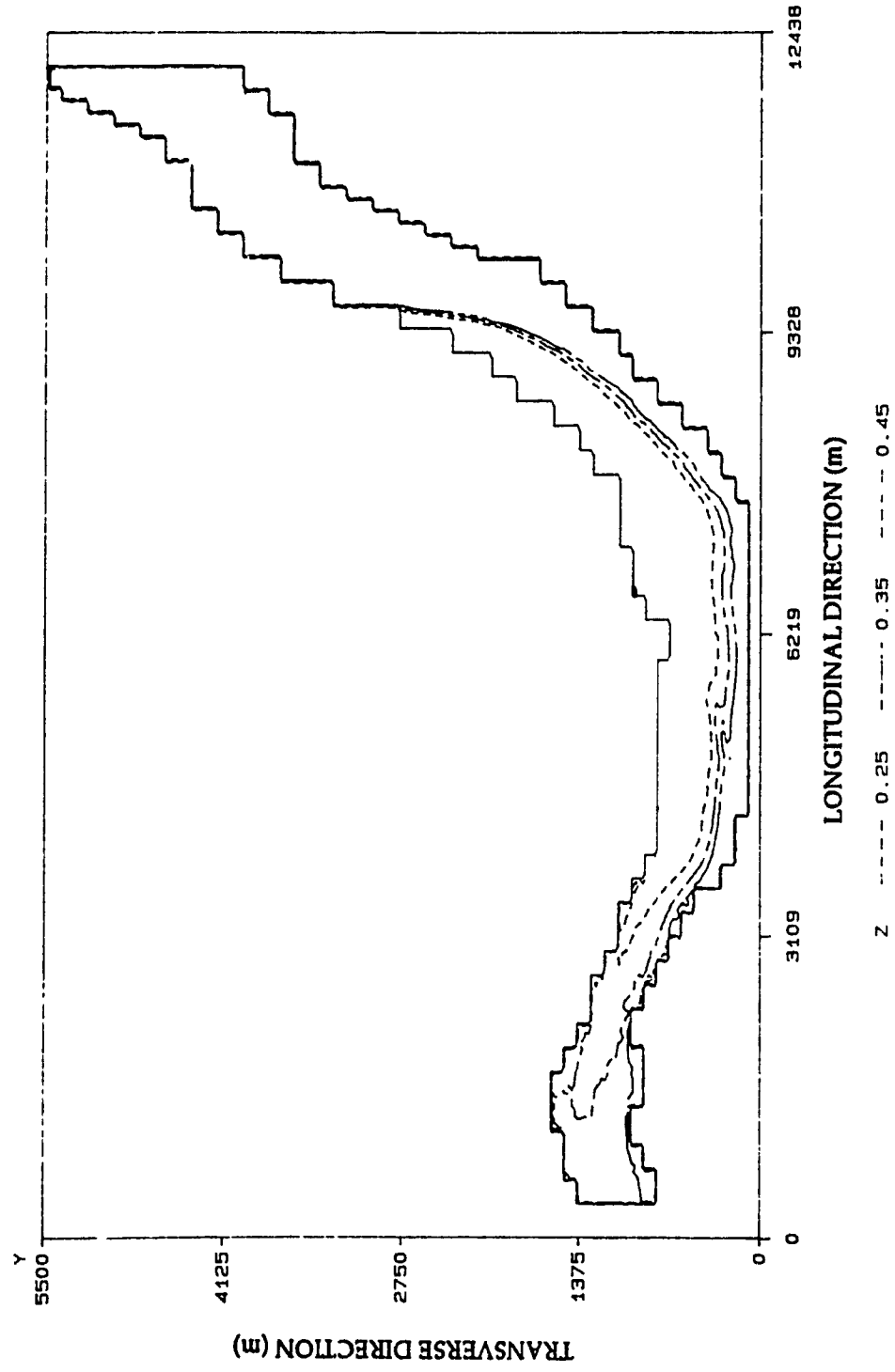

Fig. 4.29 Ice thickness distribution from Colburn equation

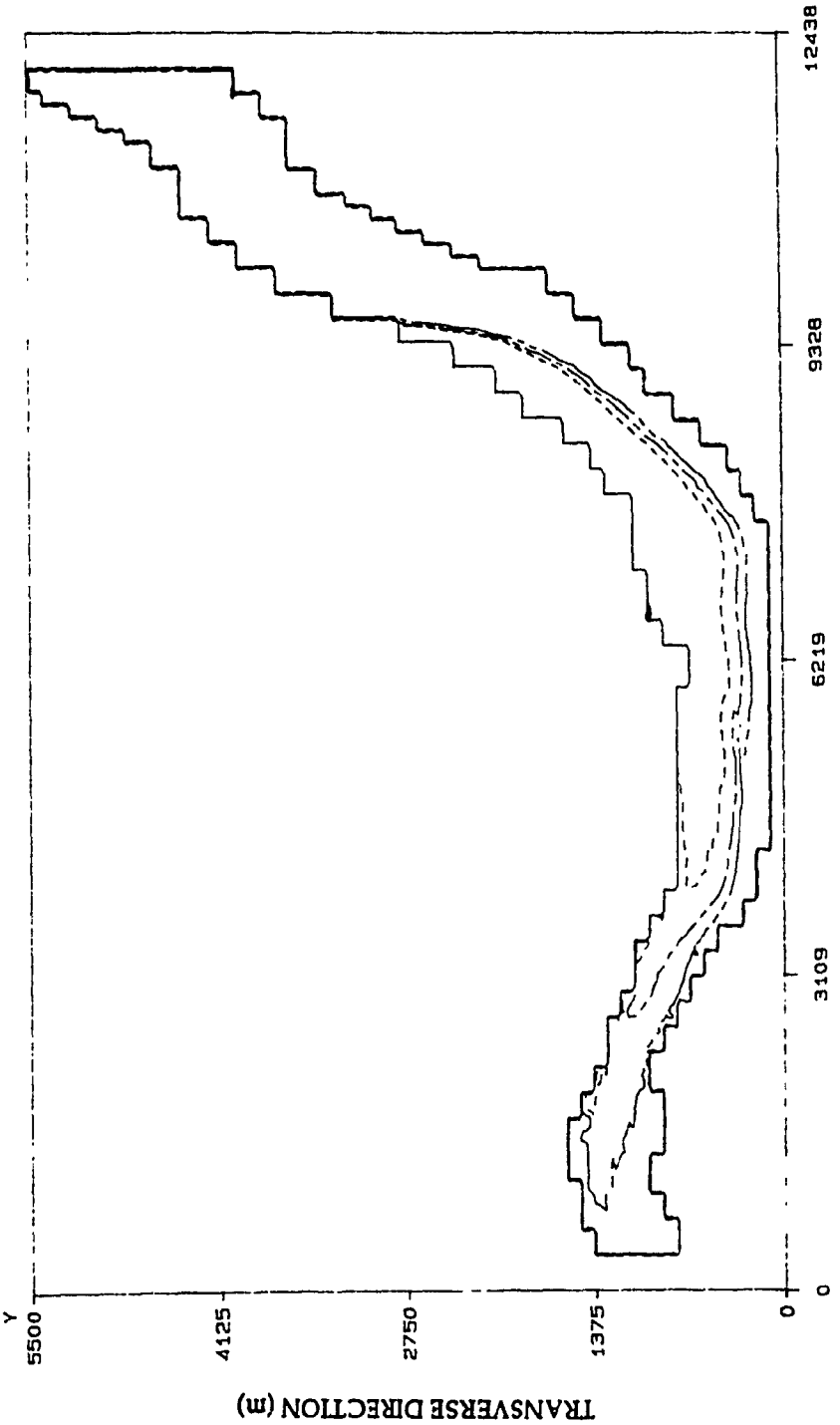

Fig. 4.30 Ice thickness distribution from Petukhov-Popov equation

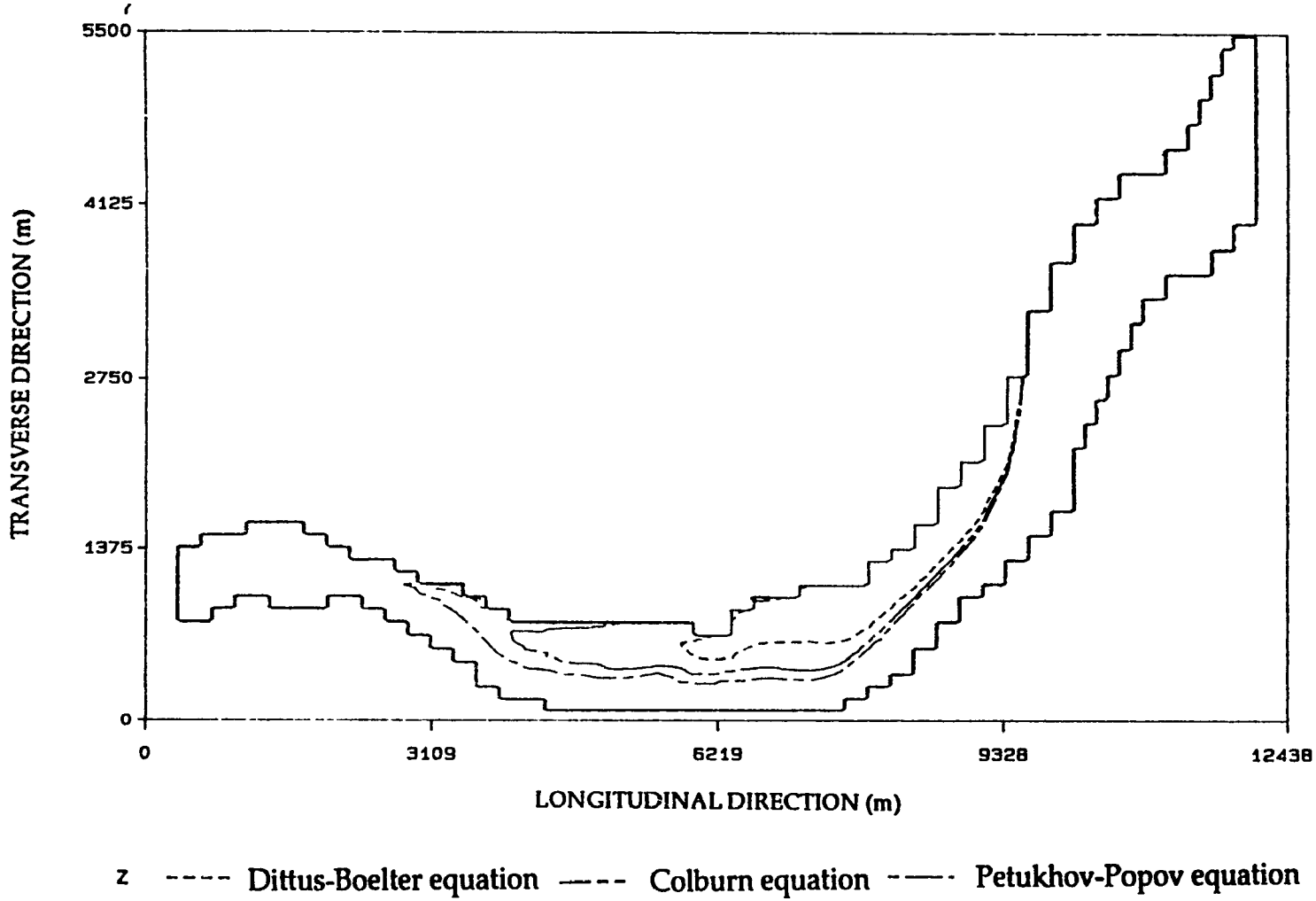

Fig. 4.31 Contour line of 0.25m ice thickness from empirical equation

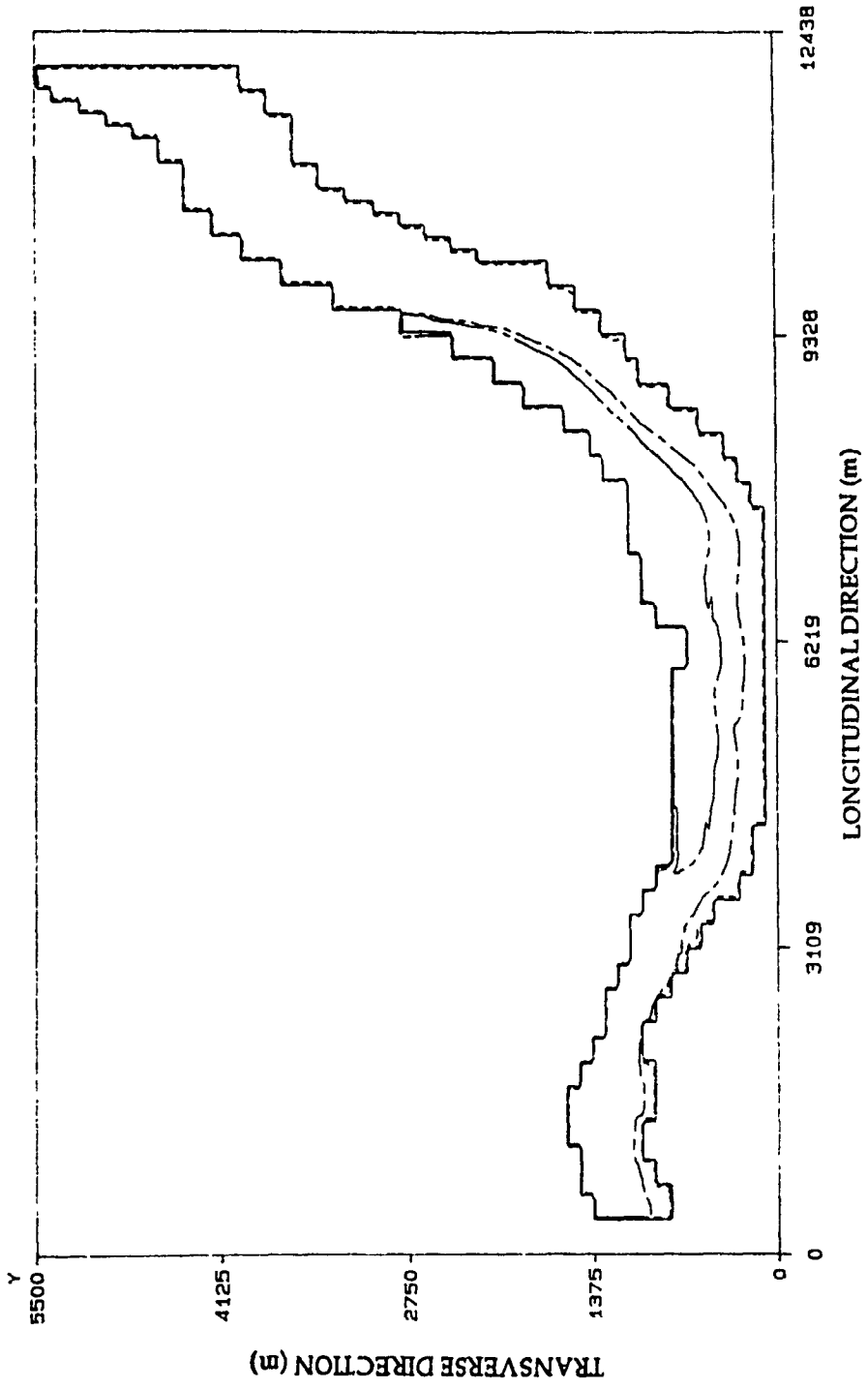

Fig. 4.32 Temperature distribution from Dittus-Boelter equation

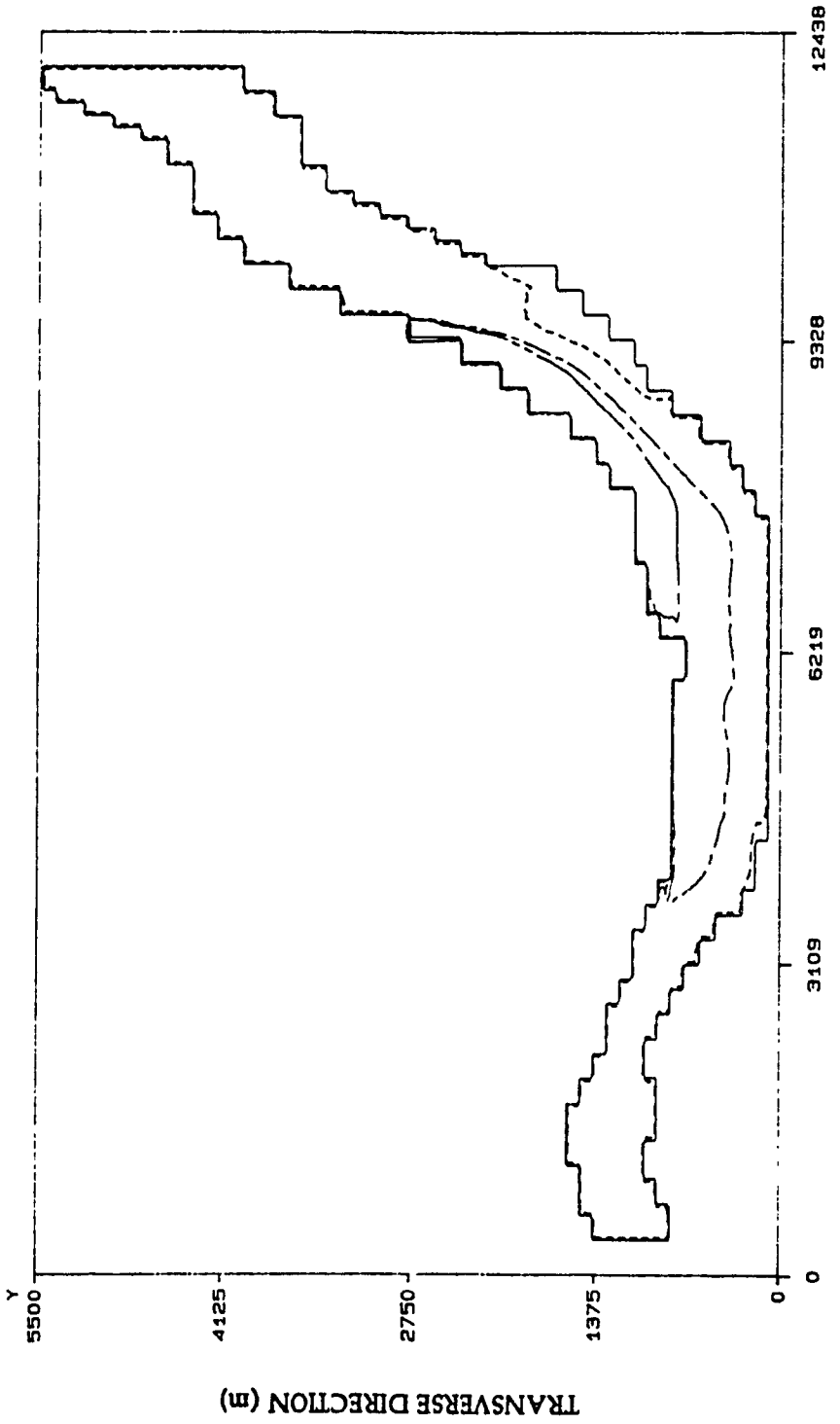

Fig. 4.33 Temperature distribution from Colburn equation

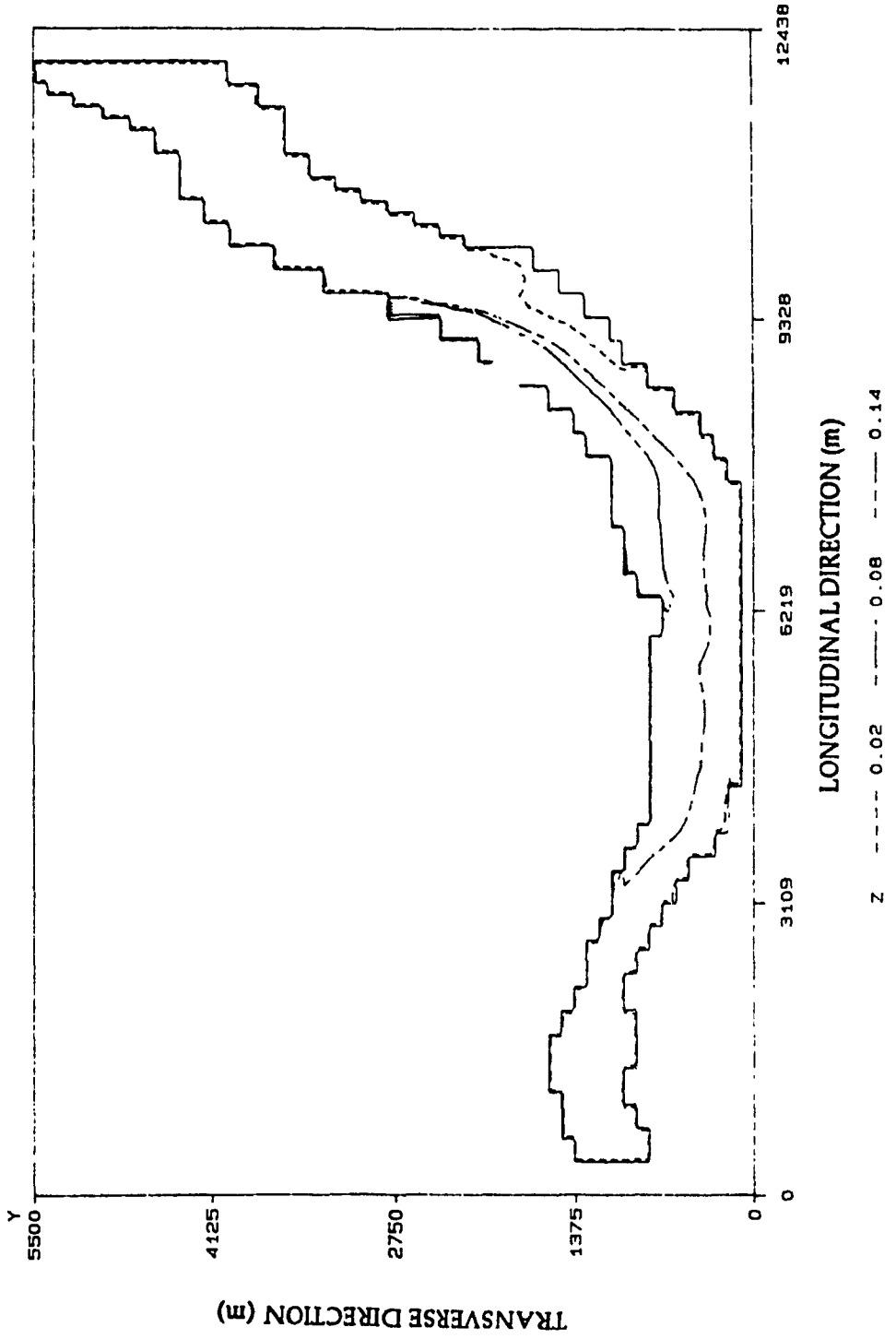

Fig. 4.34 Temperature distribution from Petukhov-Popov equation

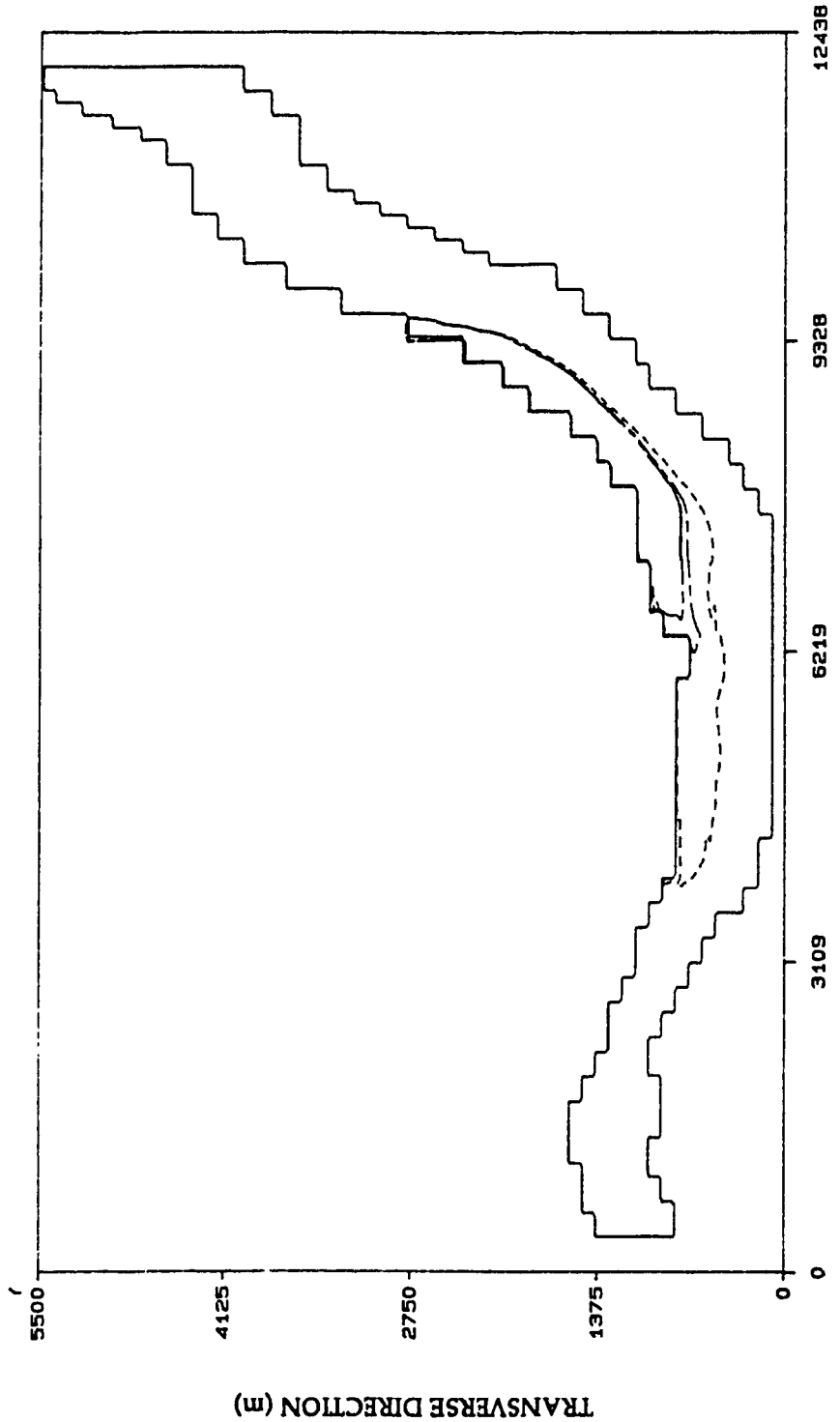

Fig. 4.35 Contour line of 0.14℃ water temperature from empirical equation

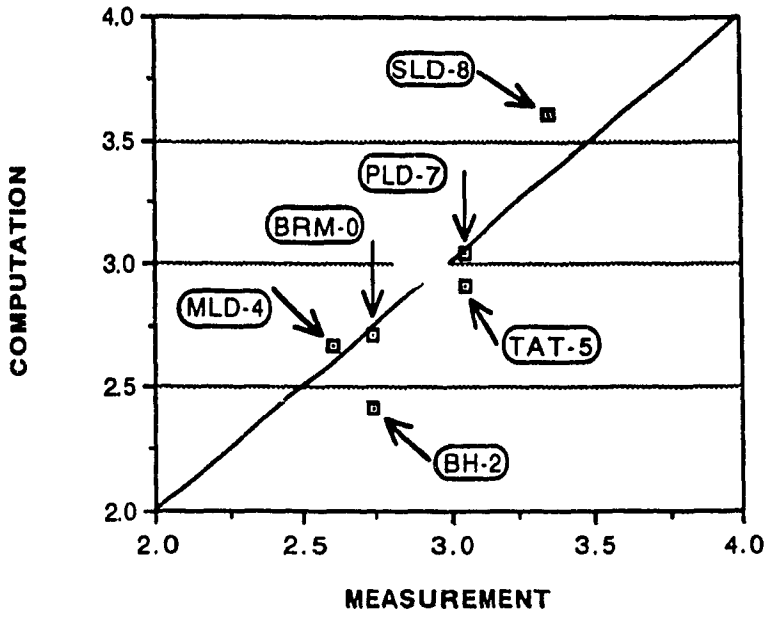

Fig. 4.36 Water depth comparison between Dittus-Boelter equation and measurement

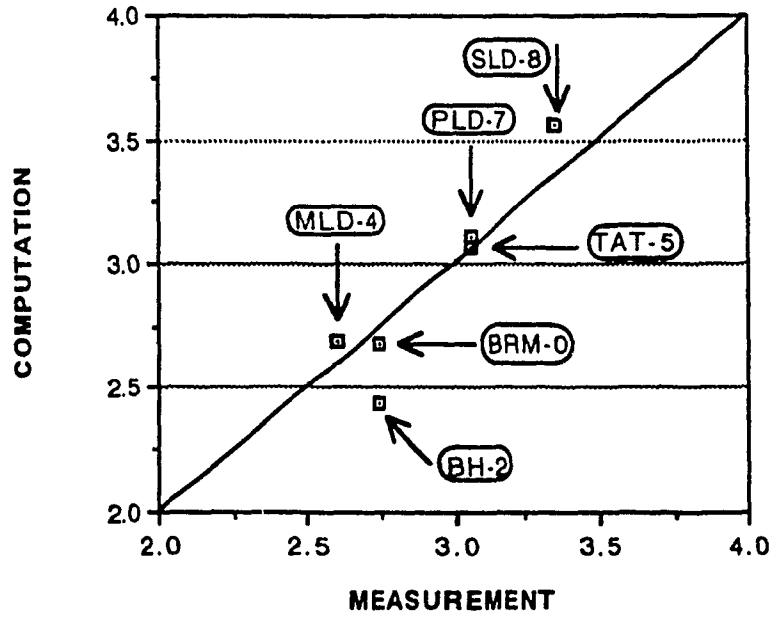

Fig. 4.37 Water depth comparison between Colburn equation and measurement

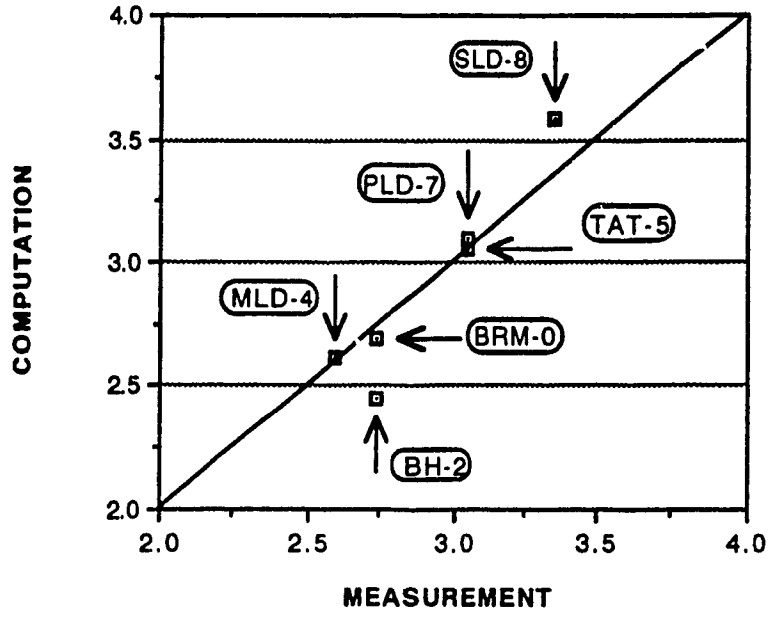

Fig. 4.38 Water depth comparison between Petukhov-Popov equation and measurement

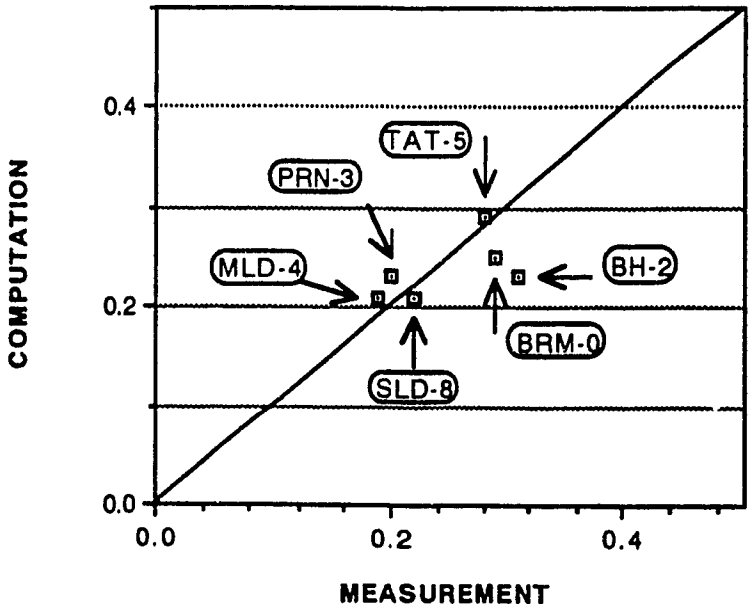

Fig. 4.39 Water velocity comparison between Dittus-Boelter equation and measurement

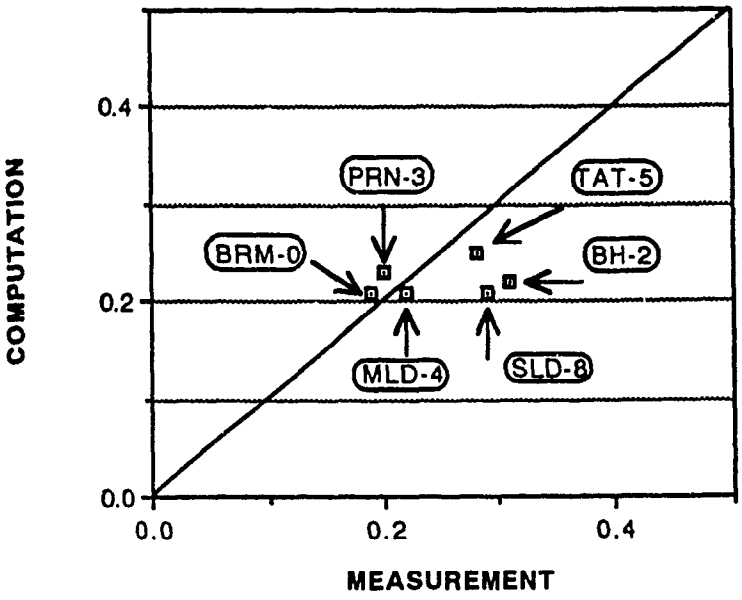

Fig. 4.40 Water velocity comparison between Colburn equation and measurement

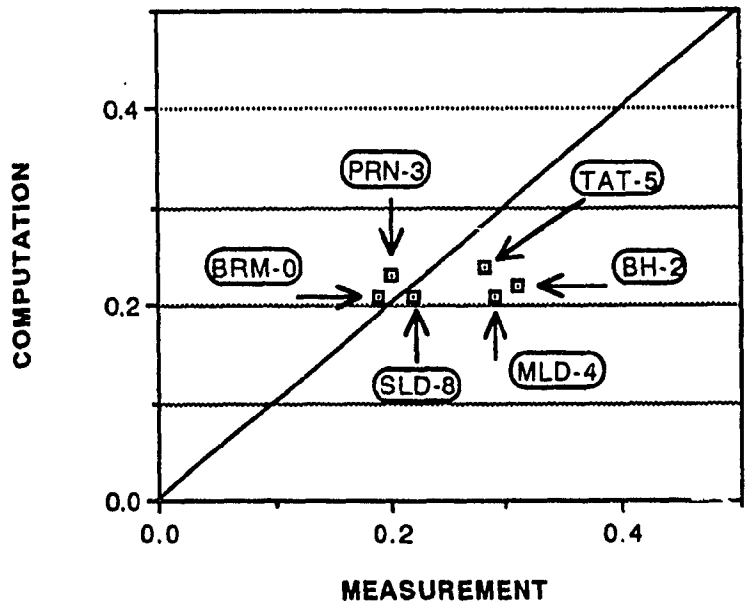

Fig. 4.41 Water velocity comparison between Petukhov-Popov equation and measurement

CHAPTER 5

CONCLUSIONS

A new formula, based on Reynolds-Colburn analogy for the computation of heat transfer coefficient at the water-ice interface, has been derived in order to get accurate ice melting prediction in the entrance region of the ice cover by using a numerical model. This new formula was used successfully in a two-dimensional numerical model to predict ice melting in the entry region. Computational results showed that the new formula had a very good agreement with experimental observations (Hewlett, 1976).

Three empirical formulas, the Dittus-Boelter, the Colburn and the Petukhov-Popov equations have been employed to generate the heat transfer coefficient for the prediction of ice melting in order to compare their effects on melting the ice cover. A comparison with the new correlation was also undertaken in the study to compare its effects in the entry region. The modeling results using these empirical formulas showed that both the Colburn equation and the Petukhov-Popov equation yielded higher values of the heat transfer coefficient than the Dittus-Boelter equation. This is due to the influence of roughness term in these two equations. The three equations produced only constant values of heat transfer coefficient, in contrast to the new formula which generated a variable heat transfer coefficient.

Conclusion can, therefore, be drawn that in numerical modeling of the ice cover melting in the entry region, it is important to use a varying heat transfer coefficient. The three empirical equations commonly used in predicting the heat transfer coefficient in modeling of ice cover melting only apply to the fully developed flow. One may obtain different results of the ice melting by adapting different formulas.

Further research is needed to confirm the computational results by experimental work. Particular attention can be given on the effect of surface roughness on melting rate in the entry region.

REFERENCES

Anderson, D.A., Tannehill, J.C. and Pletcher, R.H. (1984), Computational fluid mechanics and heat transfer, McGraw-Hill Book Company, Inc.

Ashton, G.D. (1979), "Suppression of river ice by thermal effluents", CRREL Report 79-30, U.S. Army Cold Regions Research Engineering Laboratory, Hanover, N.H., Dec.

Ashton, G.D. & Kennedy, J.F. (1972), "Ripples on underside of river ice covers", ASCE, J. Hydraulics Div., HY9, Vol. 98, pp. 1603-1624.

Ashton, G.D. (1980), "Field Investigation of Mississippi River Ice Suppression", CRREL, Feb., 1980.

Ashton, G.D. (1986), River and lake ice engineering, Water Resources Publications.

Baines, W.D. (1961), "On the transfer of heat from a river to an ice sheet", Trans. Eng. Inst. Canada, 5: 27-32.

Baldwin, B.S., McCormack, R.W. and Diewart, G.S. (1975), "Numerical techniques for the solution of the compressible Navier-Stokes

equations and implementation of turbulence models", AGARD lecture series No. 73, NATO London, Eng., Feb., pp 2-1 - 2-22.

Bayley, F.J., Owen, J.M. and Turner, A.B. (1972), Heat Transfer, Nelson.

Brown, Aubrey I. and Marco, S. M. (1958), Introduction to Heat Transfer, McGraw-Hill Book Company Inc.

Brun, E.A. (1975), Modern research laboratories for heat and mass transfer, Paris: Unesco Press.

Calkins, D.J. (1984), "Ice cover melting in a shallow river", Can. J. Civi. Eng., Vol.11, pp. 255-265

Chapman, Alan J. (1960), Heat transfer, The Macmillan Company.

Colburn, A.P. (1933), "A method of correlating forced convection heat transfer data and a comparison with liquid frictions", Trans. AICHE., Vol. 29, pp. 174-210.

Cowley, J.E., Lavender, S.T. (1975), "Convective heat transfer at an ice-water interface", Proc. Research Seminar thermal Regime of River Ice, N.R.C.C. Tech. Memo., No. 114, pp. 60-76.

Deissler, R. (1961), "International developments in heat transfer", International Heat transfer Conference, Part III, Colorado, USA, American Society of Mechanical Engineers.

Dingman, S.L., Weeks, W.F. and Yen, Y.C. (1967), "The effects of thermal pollution on river ice conditions, Part 1, A general method of calculation", CRREL report 206, U.S. Army Cold Regions Research Engineering Laboratory, Hanover, N.H., Dec.

Eckert, E.R.G. and Drake, R.M. (1987), Analysis of heat and mass transfer, Hemisphere Pub. Corp.

Fox, R. W. and Mcdonald, A. T. (1985), Introduction To Fluid Mechanics, John Wiley & Sons, N.Y.

Gebhart, Benjamin (1961), Heat transfer, McGraw-Hill Book Company, Inc.

Gilpin, R.R., Hiarata, T. & Cheng, K.C. (1980), "Wave formation and heat transfer at an ice-water interface in the presence of a turbulent flow", J. Fluid Mech., Vol. 99, pp. 619-640.

Gosman, A.D., Launder, B.E., and Reece, G.J. (1985), "Heat transfer and fluid flow", Computer-Aided Engineering, General Electric Company.

Grober, H., Erk, S. and Grigull, Ulrich (1961), Heat transfer, McGraw-Hill Book Company, Inc.

Henderson, F. M.(1966), Open Chennal Flow, Macmillan, N.Y.

Hartnett, J.P. (1955), "Experimental determination of the thermal entrance length for the flow of water and oil in circular pipes", Trans. ASME., Vol. 77, pp. 1211-1220.

Hewlett, B.Y. (1976), "Rate of recession of the leading edge of ice covers on open channel flows", Masters Thesis, The University of Iowa, Iowa, U.S.A.

Hsu, K. (1973), Spectral evolution of ice ripples, Ph.D. Thesis, The University of Iowa, Iowa, U.S.A.

Jakob, Max, Hawkins, George A. (1957), Element of heat transfer, New York, John Wiley & Sons, Lnc., London.

Komara, J., Sumbal, J. (1967), "Heat losses in channels with ice cover", Proc. 12th Congress of the Int. Assoc. for Hydraul. Res., 4:270-274.

Kreith, F. (1961), "The principle of heat transfer", McGraw-Hill, New York.

Lau, Y.Lam and Krishnappan, B.G. (1981), "Ice cover effects on stream flows and mixing", HY 10, Oct.

Majewski, W. (1988), "Determination of roughness coefficient of the underside of ice cover", IAHR Ice Symposium, Sapporo, Japan.

Markatos, N.C. (1986), Numerical simulation of fluid flow and heat/mass transfer processes, Springer-Verlag.

Marsh, P. (1990), "Modeling water temperature beneath river ice covers", Can. J. Civ. Eng., 17, pp. 36-44.

Marsh, P. & Prowse, T.D. (1986), "Water temperature and heat flux at the base of river ice covers", Cold Regions Science and Technology, Vol. 14, pp. 33-50.

Maykut, G.A., Untersteiner, N. (1971), Some results from a time-dependent thermodynamic model of sea ice, J. Geophys. Res., 76: 1500-1575.

Nezhikhovskiy, R.A. (1964), "Coefficients of roughness of bottom surface of slush-ice cover", Soviet Hydrology: Selected Papers, 2:127-150.

Ozisik, M. N. (1985), Heat transfer, McGraw-Hill Book Company, Inc.

Paily, P.P. and Macagno, E.O. (1974), "Thermal response of heated streams, solution by the implicit method", IIHR report No. 165, Iowa Institute of Hydraulic Research, Iowa City, Iowa, May.

Patankar, S.V. (1980), Numerical heat transfer and fluid flow, McGraw-Hill Book Company, Inc.

Petukhov, B.S. and Popov, V.N. (1963), "theoretical calculation of heat exchange and frictional resistance in turbulent flow in tubes of an incompressible fluid with variable physical properties", High Temperature, Vol. 1, pp. 69-83.

Plouffe, P. (1987), "Two-dimensional modeling of local river ice cover melting due to a side thermal effluent", Masters Thesis, Concordia University, Canada.

Pratte, B.D. (1979), "Review of flow resistance of consolidated smooth and rough ice covers", Canadian Hydrology Symposium, Vancouver, pp. 52-92.

Sarraf, S. and Saade, R. (1990), "Ice cover melting under turbulent flow condition", Computers in Engineering, ASCE. Conference, Vol. 2, Boston, USA.

Sarraf, S. and Saleh, W. (1990), "Local Melting Of Ice Cover By Thermal Side Effluent", Journal of Cold Regions Engineering, Vol. 1, No. 3, pp. 105-121.

Sarraf, S. and Zhang, X.T. (1991), "Investigation of heat transfer coefficient effect on river ice melting", annual CSCE conference, Vancouver, Canada.

Shen, H.T. and Yapa (1983), "Simulation of the St. Lawrence river ice cover thickness and breakup", Report 83-1, Department of Civil and Environmental Engineering, Clarkson College, Potsdam, N.Y. 37 pp.

Shen, T.S. and Chiang, L. (1984), "Simulation of growth and decay of river ice cover", Journal of Hydraulic Engineering, ASCE., Vol. 110, No. 7, July, pp. 958-971.

Sieder, E.N., Tate, G.E. (1936), "Heat Transfer and Pressure Drop of Liquids in Tubes", Ind. Eng. Chem., 28: 1429-1435.

Tsang, G., Beltaos, S. (1980), Resistance of Beauharnois Canada in winter, Proceeding of workshop on hydraulic resistance of river ice, Environment Canada, Burlington.

Wake, a. and Rumer, R.R. (1979), "Modeling the ice regime of Lake Erie", Journal of Hydraulics Div., 105: 827-844.

Wankiewicz, A. (1984), "Analysis of winter heat flow in an ice-covered Arctic stream", Can. Jour. Civil Eng., Vol. 11, pp. 430-443.

White, Frank M. (1984), Heat and Mass Transfer, Addison-Wesley Publishing Company.